Approaching the Basis Set Limit in Gaussian-Orbital-Based Periodic Calculations with Transferability: Performance of Pure Density Functionals for Simple Semiconductors

Joonho Lee,[1, a)] Xintian Feng,[2] Leonardo A. Cunha,[3] Jérôme F. Gonthier,[3] Evgeny Epifanovsky,[2] and Martin Head-Gordon[3]

[1)] *Department of Chemistry, Columbia University, New York, NY, USA*
[2)] *Q-Chem Inc., Pleasanton, CA, USA*
[3)] *Department of Chemistry, University of California, Berkeley, CA, USA*

Simulating solids with quantum chemistry methods and Gaussian-type orbitals (GTOs) has been gaining popularity. Nonetheless, there are few systematic studies that assess the basis set incompleteness error (BSIE) in these GTO-based simulations over a variety of solids. In this work, we report a GTO-based implementation for solids, and apply it to address the basis set convergence issue. We employ a simple strategy to generate large uncontracted (unc) GTO basis sets, that we call the unc-def2-GTH sets. These basis sets exhibit systematic improvement towards the basis set limit as well as good transferability based on application to a total of 43 simple semiconductors. Most notably, we found the BSIE of unc-def2-QZVP-GTH to be smaller than 0.7 mE_h per atom in total energies and 20 meV in band gaps for all systems considered here. Using unc-def2-QZVP-GTH, we report band gap benchmarks of a combinatorially designed meta generalized gradient functional (mGGA), B97M-rV, and show that B97M-rV performs similarly (a root-mean-square-deviation (RMSD) of 1.18 eV) to other modern mGGA functionals, M06-L (1.26 eV), MN15-L (1.29 eV), and SCAN (1.20 eV). This represents a clear improvement over older pure functionals such as LDA (1.71 eV) and PBE (1.49 eV) though all these mGGAs are still far from being quantitatively accurate. We also provide several cautionary notes on the use of our uncontracted bases and on future research on GTO basis set development for solids.

I. INTRODUCTION

Condensed phase simulations using quantum chemistry tools originally developed for molecules have gained popularity over many years,[1–9] with the hope of enabling development of new systematically improvable tools that can go beyond standard density functional approaches,[10] as well as existing Green's function methods[11,12] in the field. These simulations can be broadly categorized into two classes: (1) large Γ-point calculations to describe spatial inhomegeniety as found in gas, liquid, and surface simulations and (2) calculations with a relatively small unit cell and a large number of **k**-points as relevant for simulations of solids. The former category resembles large cluster calculations that are routinely performed in the molecular community and the use of Gaussian-type orbitals (GTOs) as a computational basis is not uncommon and numerically well-behaved. The use of GTOs to reach the thermodynamic limit (TDL) of (dense) solids often faces numerical difficulties associated with overcompleteness of GTOs that leads to a severe linear dependency among basis functions towards the TDL.[13–16] Nonetheless, many studies have employed Gaussian basis sets either using those developed for molecular calculations, those developed for periodic mean-field calculations,[15–18] or those optimized system-specifically without much in the way of transferability guarantees.[19–21] The use of GTOs for solid-state calcu-

lations has been growing as well exemplified by many existing GTO-based quantum chemistry programs with the periodic boundary condition capability.[22–30]

The development of compact GTO basis sets[31,32] has a long history in molecular quantum chemistry.[33,34] Since McWeeny's first proposal[35] and Boys' early attempt[36] to use GTOs for molecular systems, many developments on contracted Gaussian basis sets such as atomic natural orbital[37], correlation-consistent[38] and polarization-consistent[39,40] basis sets have made high-accuracy quantum chemistry calculations practical. However, these highly optimized contracted basis sets are usually not considered applicable to solids due to emerging linear dependencies.[16] In the early days of basis set development, even-tempered[41,42] and well-tempered[43] bases were explored as a means to obtain high-quality results using only primitive GTOs reducing the complications in sophisticated optimization procedures for exponents and contraction coefficients. In the even-tempered bases, one employs three parameters for each angular momentum shell l to define a set of "even-tempered" primitive GTOs by

$$\phi_{lmk}(\mathbf{r}) \propto \exp(-\zeta_{lk}r^2)r^l S_{lm}(\Omega) \qquad (1)$$

where ϕ_{lmk} is an atomic orbital, l and m are angular momentum quantum number, $S_{lm}(\Omega)$ are the real spherical harmonics at a solid angle Ω, k sets the total number of primitive GTOs for l, m, and ζ_{lk} is parameterized by a geometric series,

$$\zeta_{lk} = \alpha_l \beta_l^{k-1}, \ \ \alpha_l, \beta_l > 0, \ \ \beta_l \neq 1 \qquad (2)$$

In the well-tempered variants, a more sophisticated form

a)Electronic mail: jl5653@columbia.edu

is used for ζ_{lk}. In the even-tempered basis, one needs to pick a total of three parameters k, α_{lk}, and β_{lk}. The appropriate values may be obtained by looking at atoms and small molecules though finding these values can generally be tedious.[42] Even-tempered basis sets are generally much larger than contracted GTOs and thus they are rarely used in modern quantum chemistry calculations. Nonetheless, these bases have not yet been explored in the context of solid-state applications.

In this work, we propose an even simpler basis set generation protocol than that of even-tempered bases which does not involve any optimizations. Our procedure is to generate large uncontracted GTO bases that yield density functional theory (DFT) total energies per cell within 0.7 mE_h per atom in the unit cell from the complete basis set limit obtained by planewave (PW) basis. The idea is to take two existing GTO bases (one from the def2-series[44] and SZV-MOLOPT-SR-GTH[15]), uncontract these bases, and take the union of the resulting primitive GTOs while removing core orbitals that are treated by the underlying GTH pseudopotential. Like the even-tempered bases, our sets are much larger than typical contracted GTOs available in the literature, but they are not optimized for specific systems and/or mean-field methods so they should naturally bear transferability.

As an application of these bases, we focus on the basic goal of quantifying the basis set error of Gaussian-based DFT calculations. This goal is even more important to reach when considering correlated wavefunction calculations. However, the basis set incompleteness error (BSIE) in correlation energies can be quantified and characterized only after the underlying mean-field energy is converged to the basis set limit. The BSIE was directly quantified by employing the same pseudopotential proposed by Hutter and co-workers (called the GTH pseudopotential)[45,46] in both the new Gaussian-based program developed in this work and a PW-based code, Quantum Espresso (QE).[47]

Furthermore, we also apply our basis set to validating the performance of ten selected pure exchange-correlation (XC) functionals. These ten XC functionals consist of one local density approximation (LDA) functional,[48,49] five generalized gradient approximation (GGA) functionals (PBE,[50] PBEsol,[51] revPBE,[52] BLYP,[53,54] B97-D[55]), and four meta GGA (mGGA) functionals (SCAN,[56] M06-L,[57] MN15-L,[58] B97M-rV[59,60]). Our benchmark set has a total of 43 semiconductors where 40 of them were taken from the SC40 set[61] and the remaining 3 (LiH,[62–64] LiF,[65,66] and LiCl[65,66]) were taken from other places. The performance of LDA and PBE on the majority of these systems using GTOs was already documented in ref. 61 though the underlying BSIE of the associated GTO basis sets is unclear. Many PW-based codes including QE have LDA, GGA, and SCAN functionals available so it is not very difficult to assess their performance using PW-based codes.[47] In fact, the performance of LDA and GGA

functionals, as well as the SCAN mGGA, is relatively well understood for band gap problems.[67,68] However, the recently developed functionals that were combinatorially optimized for main group molecular chemistry, ωB97X-V,[69] ωB97M-V,[70] and B97M-V,[59,60] have rarely appeared in condensed phase studies[71–75] and are relatively less common and less used in PW-based codes. The same is true for the Minnesota functionals (M06-L and MN15-L). Replacing the -V tail with the -rV tail (the rVV10 van der Waals (vdW) correction[76] instead of the VV10 vdW correction[77]), an efficient implementation of the -rV tail is now available in some planewave-based codes.[47] Aside from the computational cost associated with the long-range exact exchange, an efficient implementation of these functionals should be readily possible. These combinatorially optimized functionals were found to be statistically the best XC functionals at each rung of Jacob's ladder for main group chemistry problems,[78] and they have performed very well in other molecular benchmarks also.[79,80] In the condensed phase, the mGGA, B97M-rV appears to describe properties of liquid water as accurately as far more computationally demanding hybrid functions.[72] However, the performance of B97M-rV for band gap problems is largely unknown at present. Motivated by this, we report the performance of B97M-rV for band gaps here.

This paper is organized as follows: (1) we first review basic formalisms of periodic mean-field calculations, the gaussian planewave (GPW) density fitting scheme, and an efficient implementation of rVV10, (2) we then describe our strategies for generating transferable GTO bases for simulating solids towards the TDL, (3) we discuss computational details, (4) we present results for basis set convergence of DFT total energies and band gaps using the proposed bases, (5) we assess the performance of pure XC functionals comparing against experimental band gaps, (6) we deliver cautionary notes on using our bases and on the future basis set development for solids featuring striking failures of existing GTH bases, and (7) we then conclude.

II. THEORY

Periodic mean-field calculations using a linear combination of atomic orbitals have been well-documented in many places.[81,82] Nonetheless, we aim to give a pedagogical review of the relevant theories on periodic DFT calculations within the GPW implementation and the implementation of rVV10 since these are the key compute kernels in our new implementation. Experienced readers may skip some of the subsequent sections and start from Section II D.

A. Periodic Mean-Field Calculations

As a consequence of real-space translational symmetry, crystal momentum ($\mathbf{k}$) is a good quantum number. Periodic mean-field (PMF) calculations with GTOs are hence done with crystalline molecular orbitals (CMOs), $\{\psi_i^{\mathbf{k}}\}$,[83]

$$\psi_i^{\mathbf{k}}(\mathbf{r}) = \sum_\mu C_{\mu i}^{\mathbf{k}} \phi_\mu^{\mathbf{k}}(\mathbf{r}) \qquad (3)$$

where crystalline atomic orbitals (CAOs) are defined with a lattice summation,

$$\phi_\mu^{\mathbf{k}}(\mathbf{r}) = \sum_{\mathbf{R}} \phi_\mu^{\mathbf{R}}(\mathbf{r}) e^{i\mathbf{k}\cdot\mathbf{R}} \qquad (4)$$

where $\mathbf{R}$ denotes a lattice vector represented by a sum of integer multiples of primitive vectors of the direct lattice. In PMF calculations, analogously to their molecular counterparts, the PMF energy is minimized when the CMO coefficient matrix obeys a self-consistent Roothaan-Hall equation,

$$\mathbf{F}^{\mathbf{k}} \mathbf{C}^{\mathbf{k}} = \mathbf{S}^{\mathbf{k}} \mathbf{C}^{\mathbf{k}} \epsilon^{\mathbf{k}} \qquad (5)$$

where $\mathbf{F}^{\mathbf{k}}$ is the Fock matrix at $\mathbf{k}$, $\mathbf{S}^{\mathbf{k}}$ is the overlap matrix of CAOs at $\mathbf{k}$ defined as

$$S_{\mu\nu}^{\mathbf{k}} = \sum_{\mathbf{R}} \langle \phi_\mu^{\mathbf{0}} | \phi_\nu^{\mathbf{R}} \rangle e^{i\mathbf{k}\cdot\mathbf{R}} = \sum_{\mathbf{R}} S_{\mu\nu}^{\mathbf{0R}} e^{i\mathbf{k}\cdot\mathbf{R}}, \qquad (6)$$

and $\epsilon^{\mathbf{k}}$ is the band energy at $\mathbf{k}$.

In periodic calculations with GTOs, it is very common to observe linear dependencies of the CAOs which makes the metric (overlap) matrix $\mathbf{S}^{\mathbf{k}}$ poorly conditioned. Within finite precision computer arithmetic, the resulting truncation error in the inverse metric can lead to numerical instability, convergence issues, and non-trivial errors in the PMF energies. Therefore, handling exact and near linear dependencies is crucial in GTO-based periodic calculations especially when one attempts to get to the basis set limit where linear dependencies become progressively severe. In this work, we adopted the canonical orthogonalization procedure.[84] The canonical orthogonalization procedure is defined as follows:

1. The diagonalization of $\mathbf{S}^{\mathbf{k}}$ is performed for each $\mathbf{k}$:

$$\mathbf{S}^{\mathbf{k}} = \mathbf{U}^{\mathbf{k}} \mathbf{s}^{\mathbf{k}} (\mathbf{U}^{\mathbf{k}})^\dagger \qquad (7)$$

2. For a given threshold ϵ_{lindep}, one retains the $N_{\text{CMO}}^{\mathbf{k}}$ eigenvalues in $\mathbf{s}^{\mathbf{k}}$ above ϵ_{lindep} along with their corresponding eigenvectors. We refer these subsets of eigenvalues and eigenvectors to as $\tilde{\mathbf{s}}^{\mathbf{k}}$ and $\tilde{\mathbf{U}}^{\mathbf{k}}$, respectively.

3. We then define the orthogonalization matrix $\mathbf{X}^{\mathbf{k}}$,

$$\mathbf{X}^{\mathbf{k}} = \tilde{\mathbf{U}}^{\mathbf{k}} (\tilde{\mathbf{s}}^{\mathbf{k}})^{-1/2} \qquad (8)$$

The dimension of $\mathbf{X}^{\mathbf{k}}$ is N_{CAO}-by-$N_{\text{CMO}}^{\mathbf{k}}$ and $N_{\text{CMO}}^{\mathbf{k}}$ is the dimension of the effective variational space after removing numerical linear dependencies. We note that we then have

$$(\mathbf{X}^{\mathbf{k}})^\dagger \mathbf{S}^{\mathbf{k}} \mathbf{X}^{\mathbf{k}} = \mathbf{I}_{N_{\text{CMO}}^{\mathbf{k}}} \qquad (9)$$

The choice of ϵ_{lindep} should be made so as to balance between numerical stability (i.e., removing enough basis functions to avoid excessive roundoff error and precision loss) and quality of the resulting basis set (i.e., keeping as many basis functions as possible). We picked ϵ_{lindep} to be 10^{-6} which is the default value of our molecular computations in Q-Chem.[85,86] We note that this linear dependency threshold is chosen to be reasonable for double precision, and could be tightened up if one could afford quadruple or higher precision arithmetic.

B. Review of the GPW algorithm

The GPW density fitting algorithm was first proposed by Hutter and co-workers[87] and has been popularized via the implementation in CP2K.[29,88] The central idea of the algorithm is that one employs planewaves as the auxiliary basis set for density-fitting while using GTOs as the primary computational basis set. This strategy is particularly well-suited for solid-state calculations since periodic boundary conditions are naturally imposed and planewave density fitting can be done efficiently. While applying GPW to three-dimensional (3D) systems is the most straightforward, lower-dimensional systems (0D, 1D, and 2D) need special attention to remove spurious image-image interactions. The application of GPW was successfully carried out by Füsti-Molnár and Pulay[89,90] for molecules (i.e., 0D) where spurious image-image interactions were removed exactly by using a truncated Coulomb potential. A similar idea can be generalized to 1D and 2D.[91]

Among various terms in $\mathbf{F}^{\mathbf{k}}$, in this work, we focus on the Coulomb matrix, $\mathbf{J}^{\mathbf{k}}$, because this contribution is typically the computational bottleneck in pure DFT calculations. We want to compute the Coulomb matrix element between a basis function ϕ_μ located in a unit cell $\mathbf{R} = \mathbf{0}$ (denoted as $\phi_\mu^{\mathbf{0}}$) and a basis function ϕ_ν located in a unit cell $\mathbf{R}$ (denoted as $\phi_\nu^{\mathbf{R}}$),

$$J_{\mu\nu}^{\mathbf{0R}} \equiv \int_{\mathbf{r}} \phi_\mu^{\mathbf{0}}(\mathbf{r}) V_J(\mathbf{r}) \phi_\nu^{\mathbf{R}}(\mathbf{r})$$
$$= \sum_{\mathbf{R}'} \int_{\mathbf{r}\in\mathbf{R}'} \phi_\mu^{\mathbf{0}}(\mathbf{r}) V_J(\mathbf{r}-\mathbf{R}') \phi_\nu^{\mathbf{R}}(\mathbf{r}) \qquad (10)$$

where $V_J(\mathbf{r})$ is the Coulomb potential defined as

$$V_J(\mathbf{r}) = \int_{\mathbf{r}'} \frac{\rho(\mathbf{r}')}{\mathbf{r}-\mathbf{r}'} \qquad (11)$$

and we used the fact that $V_J(\mathbf{r})$ is periodic in the unit cell displacements. We note that $\mathbf{r} \in \mathbf{R}'$ implies that the

domain of the integration is restricted to the unit cell centered at $\mathbf{R}'$.

The evaluation of $V_J(\mathbf{r})$ can be done with $\mathcal{O}(N_g \log N_g)$ complexity via the fast Fourier transform (FFT) algorithm for discrete Fourier transform where N_g is the number of grid points within the simulation cell. In reciprocal space,

$$V_J(\mathbf{G}) = \frac{4\pi}{|\mathbf{G}|^2}\tilde{\rho}(\mathbf{G}) \tag{12}$$

where

$$\tilde{\rho}(\mathbf{G}) = \frac{1}{\Omega}\int_{\mathbf{r}}\rho(\mathbf{r})e^{i\mathbf{G}\cdot\mathbf{r}} \tag{13}$$

with Ω being the volume of the computational unit cell. Using these, the GPW algorithm computes $\mathbf{J^k}$ as follows:

1. Compute $\rho(\mathbf{r})$ within a unit cell via

$$\rho(\mathbf{r}) = \frac{1}{N_k}\sum_{\mathbf{k}}\sum_{i}\sum_{\mu\nu}C_{\mu i}^{\mathbf{k}}(C_{\nu i}^{\mathbf{k}})^*\phi_{\mu}^{\mathbf{k}}(\mathbf{r})(\phi_{\nu}^{\mathbf{k}}(\mathbf{r}))^* \tag{14}$$

where N_k is the number of k-points.

2. Fourier transform $\rho(\mathbf{r})$ to obtain $\tilde{\rho}(\mathbf{G})$. This is the "density-fitting" step using a planewave auxiliary basis set.

3. Compute the Coulomb potential in reciprocal space via Eq. (12) and inverse Fourier transform to obtain $V_J(\mathbf{r})$. Note that we ignore the $|\mathbf{G}| = 0$ component.

4. Compute $\mathbf{J^k}$ via

$$J_{\mu\nu}^{\mathbf{k}} = \int_{\mathbf{r}\in\text{U.C.}}(\phi_{\mu}^{\mathbf{k}}(\mathbf{r}))^*V_J(\mathbf{r})\phi_{\nu}^{\mathbf{k}}(\mathbf{r}) \tag{15}$$

where the quadrature is performed only within the unit cell (U.C.).

Our implementation computes $\phi_{\mu}^{\mathbf{k}}(\mathbf{r})$ once in the beginning and stores these in memory. Therefore, our GPW implementation for the J-build has $\mathcal{O}(N_k N_g)$ storage cost (due to storing $\phi_{\mu}^{\mathbf{k}}(\mathbf{r})$) and $\mathcal{O}(N_k N_g + N_g \log N_g)$ compute cost assuming sparsity of CAOs. Since N_g scales with the unit cell volume while N_k does not, this algorithm approaches $\mathcal{O}(N)$ scaling. Diagonalization is performed by dense linear algebra with $\mathcal{O}(N^3)$ scaling.

C. Summary of implementation of rVV10

Some of the more modern density functionals use the VV10 vdW correction, but the cost of evaluating VV10 scales quadratically with system size. Using ideas from the work of Román-Pérez and Soler,[92] Sabatini and others proposed an alternative functional form called rVV10[76] which can be implemented efficiently with linear complexity for planewave codes while retaining similar

accuracy as VV10. Subsequently, the use of rVV10 was verified for combinatorially optimized density functionals (B97M-V, ωB97X-V, and ωB97M-V) leading to B97M-rV, ωB97X-rV, and ωB97M-rV.[60] We are interested in investigating the performance of these combinatorially optimized functionals for band gaps so an efficient implementation of rVV10 is highly desirable.

The rVV10 energy functional reads[76,77]

$$E_{\text{rVV10}} = E_{\text{rVV10}}^{\text{local}} + E_{\text{rVV10}}^{\text{non-local}} \tag{16}$$

where the local part can be absorbed into the local density approximation terms and the non-local part poses implementational challenges with a naíve quadratic scaling cost. The non-local contribution is defined as

$$E_{\text{rVV10}}^{\text{non-local}} = \frac{1}{2}\int_{\mathbf{r}}\int_{\mathbf{r}'}\rho(\mathbf{r})\kappa(\mathbf{r})^{-3/2}\rho(\mathbf{r}')\kappa(\mathbf{r}')^{-3/2}\Phi(\mathbf{r},\mathbf{r}') \tag{17}$$

where $\rho(\mathbf{r})$ is the electron density, and the kernel $\Phi(\mathbf{r},\mathbf{r}')$ is

$$\Phi(\mathbf{r},\mathbf{r}') = \frac{-1.5}{(q(\mathbf{r})R^2 + 1)(q(\mathbf{r}')R^2 + 1)(q(\mathbf{r})R^2 + q(\mathbf{r}')R^2 + 2)} \tag{18}$$

with $R = |\mathbf{r} - \mathbf{r}'|$. The remaining terms are

$$q(\mathbf{r}) = \kappa(\mathbf{r})^{-1}\sqrt{C|\frac{\nabla\rho(\mathbf{r})}{\rho(\mathbf{r})}|^4 + \frac{4}{3}\pi\rho(\mathbf{r})}, \tag{19}$$

and

$$\kappa(\mathbf{r}) = 1.5b\pi(\frac{\rho(\mathbf{r})}{9\pi})^{1/6}. \tag{20}$$

The fixed parameters b and C are a part of the definition of each XC functional that includes the rVV10 contribution. The evaluation of this leads to an overall quadratic scaling in N_g due to its six-dimensional double integral in Eq. (17).

As discussed in ref. 92, we first use cubic splines to interpolate Φ such that

$$\Phi(\mathbf{r},\mathbf{r}') \approx \sum_{\alpha,\beta}\Phi(q_\alpha,q_\beta,R)p_\alpha(q(\mathbf{r}))p_\beta(q(\mathbf{r}')) \tag{21}$$

where q_α and q_β are interpolation points and p_α and p_β are interpolating polynomials. This makes the evaluation of Φ computationally convenient because Φ becomes a function of only $|\mathbf{r} - \mathbf{r}'|$. Its dependence on q_α and q_β is easy to handle as q_α and q_β are fixed interpolation points. The number of the interpolation points is also very manageable as it is typically set to 20.[76] We now define an intermediate,

$$\theta_\alpha(\mathbf{r}) = \rho(\mathbf{r})\kappa(\mathbf{r})^{-3/2}p_\alpha(q(\mathbf{r})) \tag{22}$$

and use it to recast the non-local energy contribution into a convolution form:

$$E_{\text{rVV10}}^{\text{non-local}} = \frac{1}{2}\sum_{\alpha,\beta}\int_{\mathbf{r}}\int_{\mathbf{r}'}\theta_\alpha(\mathbf{r})\theta_\beta(\mathbf{r}')\Phi_{\alpha\beta}(|\mathbf{r}-\mathbf{r}'|)$$

$$= \frac{1}{2}\sum_{\alpha,\beta}\int_{\mathbf{G}}\tilde{\theta}_\alpha(\mathbf{G})\tilde{\theta}_\beta(\mathbf{G})\tilde{\Phi}_{\alpha\beta}(|\mathbf{G}|) \tag{23}$$

Since $\Phi_{\alpha\beta}(|\mathbf{r} - \mathbf{r}'|) = \Phi_{\alpha\beta}(R)$ is spherically symmetric, its Fourier transform can be computed by one-dimensional Fourier-sine transformation. The values of $\tilde{\Phi}_{\alpha\beta}(|\mathbf{G}|)$ on a pre-defined set of $|\mathbf{G}|$ points can be precomputed and tabulated. These tabulated values are then used for interpolation to perform the convolution in Eq. (23) for a specific set of $|\mathbf{G}|$. We note that the convolution in Eq. (23) can be performed in $\mathcal{O}(N_g \log N_g)$ time as opposed to the quadratic-scaling runtime of the naíve algorithm. A similar approach can be used to compute the Fock matrix contribution associated with rVV10.

D. Strategies for assessing the basis set error for simple solids and generating transferable GTOs

Our goal in this work is to access the near basis set limit of pure density functionals for solids using GTOs. For this purpose, it is critical to have well-defined basis set limit reference values. A popular planewave code, Quantum Espresso (QE), also implements the GTH pseudopotential[45] developed by Hutter and co-workers, which was originally developed for use in the CP2K program.[29] We have adopted the same GTH pseudopotential for use in our code as well. This allows for a direct comparison between QE and our code, which is particularly useful because QE can converge the total energy to the basis set limit almost completely by increasing the planewave cutoff.

We considered the 40 semiconductors benchmark set (SC40) first proposed by Scuseria and co-workers[61] along with three rocksalt solids (LiH,[62–64] LiF,[65,66] LiCl[65,66]). For these compounds, all-electron GTO basis sets have been proposed but their accuracy remains largely unknown.[61] Moreover, to be used with the GTH pseudopotential, we need a basis set without core electrons. Unfortunately, the standard GTH basis set series does not have a broad coverage of the periodic table beyond its minimal basis set (SZV-GTH).[15] To access the basis set limit for a variety of solids considered in this work, we propose a simple way to generate a large basis set which yields the total energy per cell close to the basis set limit (errors smaller than 0.7 mE_h per atom for DFT calculations performed here, as will be shown later). We also note that this same strategy of uncontracting existing GTO bases can be applied to the generation of all-electron bases as well.

To generate the basis set, we follow a straightforward procedure:

1. We take the existing def2-bases and uncontract the contracted GTOs therein. We then remove GTOs with an exponent greater than 20 since they correspond to core electrons that are already covered by the GTH pseudopotential. This cutoff of 20 was empirically determined and we expect that the results are not sensitive to the precise value of the cutoff given the large size of our final basis set (see below for more discussion).

2. We take the union of these uncontracted def2 bases and the uncontracted SZV-MOLOPT-SR-GTH basis set to enhance the resolution within the minimal basis set space defined by the GTH pseudopotential. This final basis set will be referred to as unc-def2-X-GTH where X can be SVP, TZVP, QZVP, etc.

One may think that having a fixed cutoff of 20 for all elements could be unphysical because increasing the atomic number tends to increase all of GTO exponents. In our case, however, the GTOs from def2 bases with an exponent larger than the largest exponent in SZV-MOLOPT-SR-GTH belong to the core region that is already treated by the GTH pseudopotential. Inspecting the range of exponents in SZV-MOLOPT-SR-GTH basis, one finds that the largest ones are smaller than 20 with the exception of Na (23.5) and Mg (30.7) up to atomic number 86. Based on our results on solids involving Mg, the cutoff of 20 works well for this element as well. Overall, the contraction of electron density due to the increase in the nuclear charge is reflected appropriately and there is no sensitivity stemming from this cutoff. We also note that when taking the union of two bases some of the exponents can be very close in value, but for simplicity we do not remove those obvious near-linear-dependencies. Instead we let the canonical orthogonalization procedure take care of them. We report these unc-def-GTH bases (unc-def2-SVP-GTH, unc-def2-SVPD-GTH, unc-def2-TZVP-GTH, unc-def2-TZVPD-GTH, unc-def2-TZVPP-GTH, unc-def2-TZVPPD-GTH, unc-def2-QZVP-GTH, unc-def2-QZVPD-GTH, unc-def2-QZVPP-GTH, unc-def2-QZVPPD-GTH) through the Zenodo repository,[93] as well as in the text files included in the final publication.

With regard to the existing GTH-based contracted GTO basis sets, at present neither the range of Gaussian exponents nor the contraction coefficients have been specifically optimized to approach the basis set limit: rather they have been designed to offer a good trade-off between compute cost and accuracy for solid-state applications. The use of uncontracted basis functions in this work is an attempt to probe the suitability of using a broad range of Gaussian exponents and angular momenta while obtaining the contraction coefficients via variational energy minimization (i.e., the MO coefficients are the contraction coefficients in our case). As a consequence of decontraction, our proposed basis sets range from quite large to very large and are heavily linearly dependent. Nonetheless, this brute force approach will permit us to assess systematic convergence of our total energies towards the basis set limit energies obtained through QE. We emphasize that potential numerical instability issues are quite well handled by the simple canonical orthogonalization procedure.

Last but not least, we note that our Gaussian basis set generation procedure does not utilize any system-dependent parameters or optimization protocols. As evidenced by even-tempered bases,[41,42] this is particularly

important for ensuring transferability. Our exponents retain both tight exponents that are effective for condensed phase and relatively diffuse exponents that are effective for atomic (or molecular) limits. Therefore, we expect that the BSIE is relatively insensitive to the underlying geometry. Nonetheless, when atoms come too close together, GTOs are expected to perform more poorly due to the higher degree of linear dependence as will be shown later in Section V C.

III. COMPUTATIONAL DETAILS

We implemented a GPW-based periodic DFT code in a development version of Q-Chem.[85,86] Our implementation assumes overall $\mathcal{O}(N^2)$ memory storage that amounts to storing Fock, density, and CMO coefficient matrices. For the systems examined in this work, our memory strorage is dominated by keeping the GTO basis function values evaluated on the FFT grid despite its formal linear scaling based on sparsity. In the future, this practical memory bottleneck can be removed by computing these on the fly. We also note that our GPW algorithms scale linearly with the system size to produce the Fock matrix and our SCF program scales cubically with system size due to linear algebra functions such as matrix diagonalization. We control the resolution of the PW density fitting basis with a single parameter: the kinetic energy cutoff (E_{cut}). Each auxiliary basis PW can be indexed by 3 integers, (n_1, n_2, n_3) which reside on a $(2n_1^{\max} - 1) \times (2n_2^{\max} - 1) \times (2n_3^{\max} - 1)$ grid where each integer $n_i \in \{-n_i^{\max}, \cdots, n_i^{\max}\}$ with

$$n_i^{\max} = \frac{\sqrt{8E_{\mathrm{cut}}}}{||\mathbf{b}_i||} \tag{24}$$

where $\mathbf{b}_i$ denotes one of the reciprocal vectors. For our GPW calculations, we used E_{cut} of 1500 eV for everything except those that contain Ba (2000 eV) and Mg (4500 eV). The resulting density fitting error was found to be smaller than 100 μE_h per atom in the unit cell, which is negligible for the purpose of this paper.

The reference planewave basis calculations were all performed with QE where we used E_{cut} (for the wavefunction itself) of 1200 Ry for total energy calculations. For the band structure calculations, we used E_{cut} of 1200 Ry for systems containing Mg and E_{cut} of 750 Ry for everything else.

The lattice constants were fixed at experimental values[61] and experimental band gaps for the SC40 set were taken from [61]. The experimental band gaps and lattice constants of LiH, LiF, and LiCl were taken from refs. 62–66. We used the GTH-LDA pseudopotential in all calculations for both GPW and PW (through QE) calculations to enable direct comparison of total energies. We used the Monkhorst-Pack[94] $\mathbf{k}$-mesh to sample the first Brillouin zone and ensured the convergence of the total energy per cell to the TDL for all solids examined here. We found that a $6 \times 6 \times 6$ $\mathbf{k}$-mesh is enough to converge

the total energy per cell to an error of smaller than 0.1 mH for all solids considered. Therefore, for band structure calculations and cold curve calculations, we used a $6 \times 6 \times 6$ Monkhorst-Pack $\mathbf{k}$-mesh. Since the GPW implementation is also available in other open-source packages such as CP2K[29] and PySCF,[95] we also used these two packages to validate our implementation in the initial stage of this work.

We examined a total of ten XC functionals, LDA (Slater exchange[48] and PZ81 correlation[49]), PBE,[50] PBEsol,[51] revPBE,[52] BLYP,[53,54] B97-D,[55] SCAN,[56] M06-L,[57] MN15-L,[58] and B97M-rV.[59,60] For 11 solids in our benchmark set (C, Si, SiC, BN, BP, AlN, MgO, MgS, LiH, LiF, LiCl), widely used GTH basis sets[15] are available: DZVP-GTH, TZVP-GTH, TZV2P-GTH, QZV2P-GTH, and QZV3P-GTH. We therefore assessed the accuracy of those existing bases only over a smaller subset of our benchmark set, but our proposed basis sets were examined for all 43 solids considered in this work. The basis set convergence study against PW was carried out only for LDA and PBE while the overall band gap accuracy was examined for all ten functionals.

IV. RESULTS AND DISCUSSION

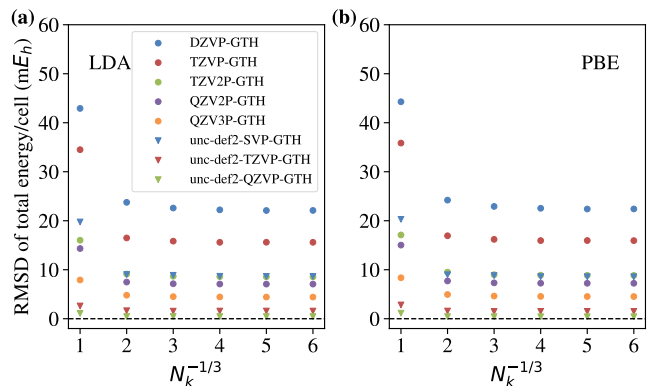### A. Basis set convergence of total DFT energies

FIG. 1. Root mean square deviation (RMSD) of DFT total energies (mE_h) per cell with respect to that of QE over 11 solids as a function of the number of $\mathbf{k}$-points for (a) LDA and (b) PBE functionals using GTH and unc-def2-GTH bases.

We first examine the subset of 11 solids for LDA and PBE functionals as presented in Fig. 1. In particular, Fig. 1 shows the root-mean-square-deviation (RMSD) of total energies compared to QE total energies (namely total energies in the basis set limit) as function of the size of the $\mathbf{k}$-mesh. $N_k = 216$ ($6 \times 6 \times 6$) is enough to reach the TDL. While smaller $\mathbf{k}$-mesh calculations such as the Γ-point only calculations are unphysical, we are interested in how the basis set error changes as a function of the $\mathbf{k}$-mesh size. Since both PW and our GTO results

share the same Hamiltonian for each size of **k**-mesh, we can assess the basis set error of GTO calculations as long as the reference PW energies are fully converged to the basis set limit. For all **k**-mesh sizes, the GTH basis set series shows systematically more accurate results relative to the basis set limit as cardinality (and the size of the basis set) increases. We note that $N_k = 1$ (just including the Γ-point) shows the largest basis set error in all examples considered here. This is because the local expressive power of GTOs also increases as one increases the size of **k**-mesh due to the non-orthogonality of GTOs. While the systematic improvement of GTH bases is very appealing, we note that the residual basis set error with QZV3P-GTH is still about 5 mE_h which is quite large considering how small the simulation cells are (2 or 4 atoms total).

The unc-def2-GTH basis series also shows a systematic improvement with cardinal number, with much smaller errors than the corresponding contracted GTH basis results. As an example, the performance of unc-def2-SVP-GTH is nearly on par with TZV2P-GTH except at the Γ-point. The larger bases, unc-def2-TZVP-GTH and unc-def2-QZVP-GTH, both perform excellently on this set, including the Γ-point result. In particular, unc-def2-QZVP-GTH is able to deliver total energies in the TDL that are all within 1 mE_h of the basis set limit. This shows the completeness of our proposed bases though of course these are much bigger in size than standard GTH bases, and therefore far more computationally demanding. We provide more detailed information on selected elements in Section V A. Finally, we note that Fig. 1 (a) for LDA and (b) for PBE show virtually no difference, which suggests that our conclusions do not depend on functional (of course functionals that depend particularly strongly on fine details of the density may be far harder to converge to the basis set limit using GTOs[96]).
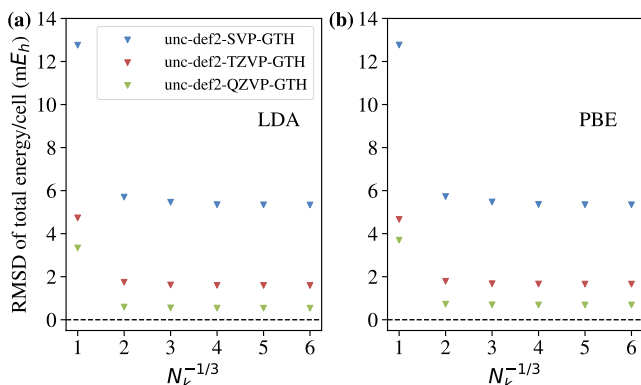

FIG. 2. Root mean square deviation (RMSD) of DFT total energies (mE_h) per cell with respect to that of QE over 43 solids as a function of the number of **k**-points for (a) LDA and (b) PBE functionals using unc-def2-GTH bases.

In Fig. 2, we repeat the same analysis but over the entire benchmark set of 43 solids. As before, unc-def2-

GTH bases struggle for $N_k = 1$ but work well for larger **k**-meshes. RMSD systematically decreases as we increase the size of the basis set. With the largest basis set, unc-def2-QZVP-GTH, we achieve better than 1 mE_h accuracy in the TDL for the LDA and PBE functionals, as measured by the RMSD values. Systems with the largest error in the TDL are SrSe (1.2 mE_h) in the case of LDA and GaP (1.4 mE_h) in the case of PBE. As observed in the case of even-tempered bases, we expect that the result can be systematically made better by adding more exponents and increasing the maximum angular momentum.[41,42] For instance, in the case of SrSe/LDA, employing unc-def2-QZVPP-GTH (adding two additional f functions to both Sr and Se), we observe an error of 0.4 mE_h which is three times smaller than that of unc-def2-QZVP-GTH. While we can obtain overall better results by using unc-def2-QZVPP-GTH, we will mainly focus on the use of the unc-def2-QZVP-GTH basis set for the rest of the paper for simplicity. In summary, these benchmark calculations suggest that unc-def2-GTH basis sets can achieve near basis set limit DFT total energies reliably towards the TDL. This result implies that the range of exponents and angular momenta in our bases is quite appropriate for solids.

B. Basis set convergence of DFT band gaps

In many materials applications, DFT calculations are used not just to compute the ground state energy but to obtain spectral information through Kohn-Sham orbital energies.[67] In doing so, one uses information from virtual orbitals in addition to that from occupied orbitals. In the case of total energies presented in Section IV A, only occupied orbitals affect the results. Here, we are assessing the quality of the difference between the lowest energy virtual orbital (i.e., the conduction band minimum) and the higher energy occupied orbital. It is possible that some BSIEs may cancel when taking energy differences.

In Fig. 3, we present the RMSD of band gaps using GTO bases compared to the basis set limit results for LDA and PBE functionals. To compare unc-def2-GTH bases with GTH bases, we limit ourselves to the subset of 11 solids for the time being. Somewhat surprisingly, we observe almost no improvement in the band gap when going from DZVP-GTH to TZVP-GTH. By contrast, Fig. 1 shows a reduction in the RMSD of total energies of about 8 mE_h when increasing the basis set size from DZVP-GTH to TZVP-GTH. However, this total energy improvement does not result in any band gap improvement. Nonetheless, past TZVP-GTH, the GTH bases do show systematic improvement in the band gap estimation. With the largest GTH basis set (QZV3P-GTH), RMSD in the band gap is 18-20 meV depending on the XC functional. Consistent with the total energy benchmark presented in Section IV A, unc-def2-GTH bases also exhibit systematic improvement. While the quality of unc-def2-SVP-GTH was on par with TZV2P-GTH in
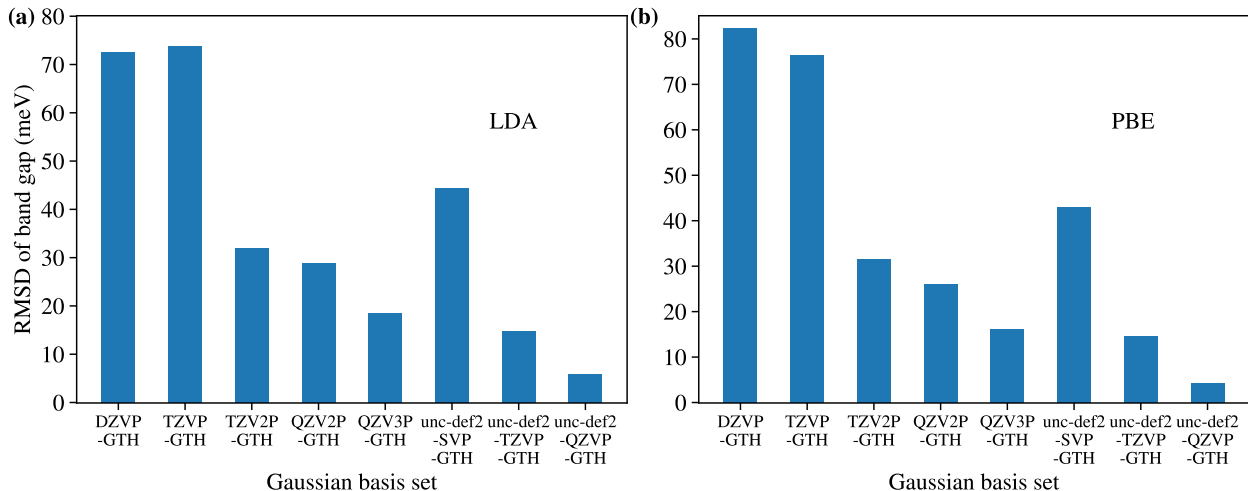
FIG. 3. Root mean square deviation (RMSD) of DFT band gaps (meV) with respect to those of QE over 11 solids (a) LDA and (b) PBE functionals using GTH and unc-def2-GTH bases.

Fig. 1, its band gap is clearly worse than that of TZV2P-GTH highlighting favorable error cancellation in TZV2P-GTH. Nonetheless, unc-def2-TZVP-GTH is similar to QZV3P-GTH and unc-def2-QZVP-GTH has RMSD of 5.8 meV and 4.2 meV, respectively for LDA and PBE, showing its ability to converge band gaps to the basis set limit.
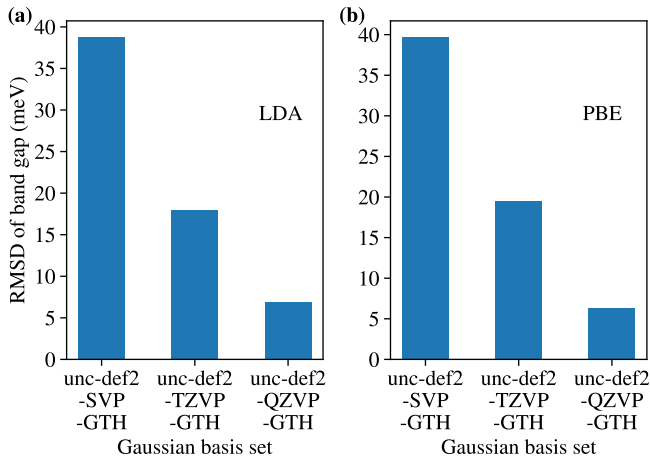

FIG. 4. Root mean square deviation (RMSD) of DFT band gaps (meV) with respect to those of QE over 43 solids (a) LDA and (b) PBE functionals using unc-def2-GTH bases.

Encouraged by these results, we also analyzed the BSIEs in band gaps over all 43 solids using unc-def2-GTH bases as presented in Fig. 4. With unc-def2-SVP-GTH, the RMSD value is about 40 meV and it becomes less than 20 meV when using unc-def2-TZVP-GTH. Lastly, with unc-def2-QZVP-GTH, the RMSD value becomes 6.9 meV and 6.3 meV, respectively, for LDA and PBE. However, we note that the largest deviation is about 20 meV

in both functionals, which corresponds to the band gap of SrSe. SrSe is the system with the largest total energy error for LDA as noted in the discussion of Fig. 2 in Section IV A. Again, this remaining error can be further reduced by adding more GTOs to unc-def2-QZVP-GTH (e.g., using unc-def2-QZVPP-GTH), but we do not pursue this here. The central message of this section is that the BSIE in the band gap reported in this paper using unc-def2-QZVP-GTH is smaller than 20 meV based on the numerical data. This is about 50 times smaller than the intrinsic errors in standard functionals for band gaps, so unc-def2-QZVP-GTH should be suitable for benchmarking purposes.

C. Performance of pure DFT functionals

Having established the accuracy of unc-def2-GTH bases, we assess the performance of pure DFT functionals over these simple solids. Unfortunately, some of the 43 solids considered here do not have experimental band gaps. These solids are BSb, CaS, CaSe, CaTe, SrS, SrSe, and SrTe. Leaving aside these seven cases, we have a total of 36 experimental band gaps. unc-def2-QZVP-GTH is used with all XC functionals considered in this section. The DFT band gaps over 43 solids along with the available experimental gaps are presented in Table I. For an overall summary, it may be more instructuve to look at statistics of the band gap results as shown in Fig. 5. Looking at the mean-average-deviation (MAD), it is immediately evident that all pure functionals examined here exhibit the infamous band gap underestimation problem of pure functionals.[67] Nonetheless, one can still find systematic improvement for going from the simplest functional, LDA, to more modern meta GGA functionals, SCAN, M06-L, MN15-L, and B97M-rV in terms of

	LDA	PBE	PBEsol	revPBE	BLYP	B97-D	SCAN	M06-L	MN15-L	B97M-rV	Exp.
C	4.12	4.33	4.16	4.38	4.60	4.57	4.64	4.84	4.24	4.67	5.48
Si	0.49	0.66	0.52	0.72	0.94	0.91	0.93	1.12	0.96	0.92	1.17
Ge	0.00	0.00	0.00	0.00	0.00	0.00	0.20	0.46	0.43	0.26	0.74
SiC	1.33	1.50	1.35	1.54	1.85	1.95	1.81	1.83	1.92	2.07	2.42
BN	4.36	4.64	4.42	4.71	5.03	5.07	5.03	4.94	4.98	5.28	6.22
BP	1.20	1.38	1.23	1.42	1.66	1.62	1.67	1.95	1.61	1.70	2.4
BAs	1.16	1.34	1.19	1.40	1.60	1.59	1.57	1.85	1.55	1.66	1.46
BSb	0.76	0.91	0.78	0.96	1.15	1.17	1.06	1.21	1.08	1.15	N/A
AlP	1.47	1.67	1.50	1.75	1.98	2.04	1.99	2.20	2.12	2.16	2.51
AlAs	1.36	1.58	1.40	1.66	1.89	1.95	1.86	2.00	1.99	2.03	2.23
AlSb	1.17	1.36	1.20	1.45	1.57	1.58	1.56	1.78	1.63	1.63	1.68
bGaN	1.61	1.79	1.68	1.85	1.86	1.96	1.86	1.88	1.43	1.86	3.3
GaP	1.44	1.66	1.50	1.75	1.70	1.72	1.85	1.89	1.84	2.05	2.35
GaAs	0.29	0.51	0.41	0.58	0.44	0.46	0.62	0.92	0.72	1.01	1.52
GaSb	0.00	0.17	0.08	0.23	0.08	0.08	0.21	0.50	0.36	0.64	0.73
InP	0.42	0.61	0.52	0.68	0.57	0.56	0.57	0.86	0.36	0.88	1.42
InAs	0.00	0.00	0.00	0.00	0.00	0.00	0.00	0.00	0.00	0.03	0.41
InSb	0.00	0.00	0.00	0.00	0.00	0.00	0.00	0.00	0.00	0.13	0.23
ZnS	1.80	2.12	1.94	2.24	2.15	2.24	2.38	2.56	2.00	2.36	3.66
ZnSe	1.01	1.33	1.15	1.45	1.35	1.43	1.60	1.80	1.31	1.67	2.7
ZnTe	1.07	1.38	1.22	1.49	1.38	1.43	1.60	1.83	1.40	1.79	2.38
CdS	0.85	1.15	0.98	1.27	1.16	1.22	1.22	1.34	0.77	1.23	2.55
CdSe	0.34	0.64	0.48	0.76	0.66	0.70	0.72	0.88	0.34	0.82	1.9
CdTe	0.52	0.81	0.66	0.93	0.81	0.82	0.84	1.07	0.52	1.06	1.92
MgS	3.27	3.57	3.39	3.73	3.71	3.88	4.14	4.03	4.06	4.17	5.4
MgTe	2.30	2.59	2.43	2.75	2.72	2.89	3.16	3.18	2.99	3.23	3.6
MgO	4.68	4.93	4.79	5.06	5.17	5.49	5.59	5.01	5.69	5.55	7.22
MgSe	1.70	2.01	1.89	2.16	2.10	2.47	2.58	2.66	3.20	2.70	2.47
CaS	2.17	2.41	2.27	2.51	2.52	2.64	2.92	2.56	3.03	3.05	N/A
CaSe	1.90	2.14	2.00	2.24	2.27	2.38	2.63	2.28	2.73	2.78	N/A
CaTe	1.42	1.65	1.51	1.74	1.80	1.90	2.08	1.74	2.19	2.27	N/A
SrS	2.22	2.49	2.33	2.61	2.62	2.74	2.92	2.57	2.86	2.95	N/A
SrSe	2.01	2.28	2.12	2.40	2.43	2.54	2.69	2.35	2.63	2.74	N/A
SrTe	1.57	1.83	1.66	1.94	2.00	2.10	2.20	1.87	2.17	2.29	N/A
BaS	2.01	2.26	2.11	2.38	2.36	2.44	2.58	2.25	2.38	2.51	3.88
BaSe	1.83	2.07	1.92	2.19	2.19	2.26	2.39	2.07	2.21	2.35	3.58
BaTe	1.49	1.74	1.58	1.85	1.87	1.93	2.03	1.74	1.90	2.03	3.08
LiH	2.64	3.01	2.78	3.15	3.44	3.69	3.61	3.87	4.52	4.39	4.9
LiF	8.92	9.33	9.11	9.56	9.49	9.92	10.08	9.64	10.27	9.77	14.2
LiCl	6.01	6.40	6.18	6.61	6.56	6.83	7.21	7.08	7.48	7.22	9.4
AlN	4.25	4.38	4.25	4.43	4.66	4.78	4.87	4.75	4.94	5.24	6.13
GaN	1.86	2.05	1.94	2.12	2.12	2.21	2.12	2.13	1.68	2.11	3.5
InN	0.00	0.00	0.00	0.01	0.00	0.04	0.00	0.00	0.00	0.00	0.69
RMSD	1.72	1.50	1.64	1.41	1.39	1.28	1.20	1.26	1.27	1.17	N/A
MAD	-1.46	-1.23	-1.37	-1.14	-1.10	-1.02	-0.95	-0.90	-0.99	-0.84	N/A
MAX	5.28	4.87	5.09	4.64	4.71	4.28	4.12	4.56	3.93	4.43	N/A

TABLE I. Experimental and theoretical band gaps (or fundamental gaps) (eV) from various functionals over 43 solids. N/A means "not available". RMSD, MAD, and MAX denote, respectively, root-mean-square-deviation, mean-average-deviation, and maximum deviation in reference to experimental values. We took experimental references for three rocksalt solids (LiH,LiF,LiCl) from refs 62–64, 65,66, and 65,66, respectively. The rest of experimental values were taken from ref. 61.

the root-mean-square-deviation (RMSD) values. While the performance of B97M-rV is not great for those band gaps, it still stays as one of the more accurate pure functionals for these problems. This is encouraging because B97M-rV is statistically the most accurate pure XC functional in main group chemistry applications.[78] Overall, all pure functionals perform poorly in this benchmark study and the inclusion of exact exchange seems necessary. This is not a new observation on its own and has

been well-documented even for nearly the same benchmark set that we study here.[61,97] In ref. 97, the authors consider many different ways to analyze the statistical data of LDA, PBE, and PBEsol along with other hybrid functionals and revealed that hybrid functionals always perform the best in nine out of ten statistical analyses. It will be interesting to revisit this benchmark set with modern hybrid functionals in the future.

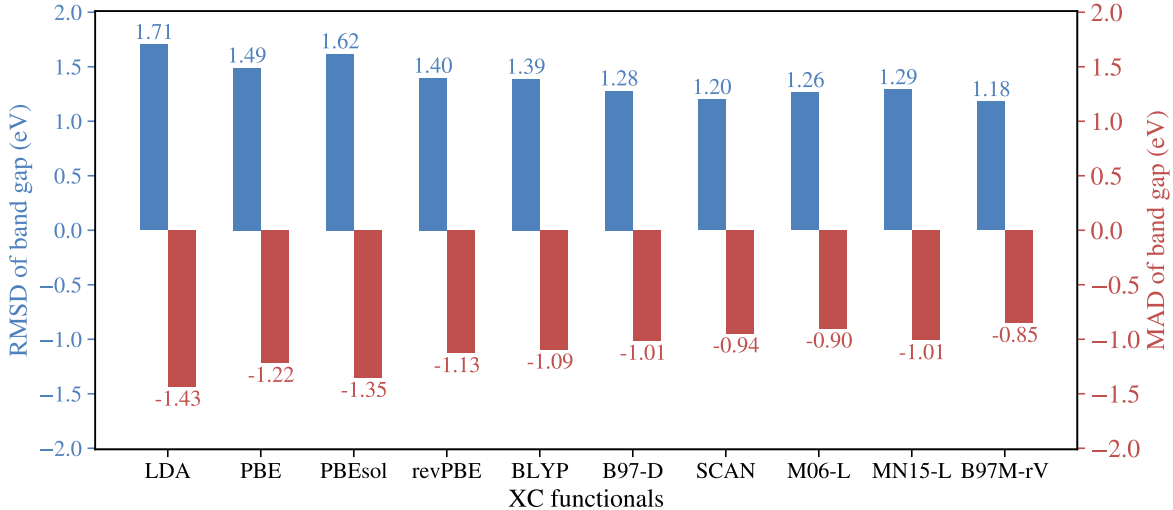For simplicity and due to the unavailability of

FIG. 5. Band gap (eV) comparison over 36 solids between DFT (ten different functionals) and experiments: Blue: root-mean-square-deviation (RMSD) of DFT band gaps (eV) with respect to those of experiments and Red: mean-average-deviation (MAD) of DFT band gaps (eV) with respect to those of experiments

functional-specific GTH pseudopotentials for most XC functionals considered here, we employed the GTH-LDA pseudopotential for all functionals in this section. Since this is not ideal, we checked the sensitivity of our conclusions with respect to the choice of the pseudopotential by testing GTH-LDA, GTH-PBE, and GTH-BLYP pseudopotentials with the BLYP functional. In all cases the RMSD and MAD are affected by less than 0.1 eV, which is a smaller energy scale than that of the band gap errors by roughly a factor of 10. For completeness, we provide the relevant numerical data in the Supplementary Material (see Table S1).In the future, all-electron calculations could be done with all-electron basis sets generated via a similar protocol presented here. Alternatively, one could generate functional-specific GTH pseudopotentials for the modern XC functionals considered here.

V.   OUTLOOK FOR FUTURE BASIS SET DESIGN

In this section, we would like to deliver cautionary notes on using our proposed bases and some discussion on future research in basis set design for solids.

A.   Our basis set is accurate but very large

While our proposed unc-def2-GTH bases are of high quality, these bases are very large due to the decontraction from the original contracted GTO bases. This large size carries a significant computational cost. This is the major drawback of even-tempered and well-tempered bases, and it is one that our unc-def2-GTH bases also share. To be more concrete, we provide the number of

	Si	C	O	Mg
SZV-GTH	4	4	4	5
DZVP-GTH	13	13	13	14
TZVP-GTH	17	17	17	18
TZV2P-GTH	22	22	22	23
QZV2P-GTH	26	26	26	27
QZV3P-GTH	31	31	31	32
unc-def2-SVP-GTH	40	41	40	53
unc-def2-TZVP-GTH	62	58	57	68
unc-def2-QZVP-GTH	90	83	81	86

TABLE II. Number of basis functions in the basis sets used in this work for selected elements (Si, C, O, and Mg).

basis functions for selected elements (Si, C, O, Mg) in Table II. unc-def2-SVP-GTH is about three times bigger than DZVP-GTH while our unc-def2-TZVP-GTH is roughly three times bigger than TZV2P-GTH. Similarly, our largest basis set unc-def2-QZVP-GTH is about 2.5–3 times larger than QZV3P-GTH.

Because of compute cost and memory demand, there is a need to compress these bases for practical calculations. Perhaps, the most difficult (but most effective if done correctly) way to compress them is to obtain transferable contraction coefficients. One could start by inspecting the molecular orbitals (or Bloch orbitals) that our calculations produce for those simple solids. Another strategy is to take these mean-field molecular orbitals and compress the virtual space for subsequent correlation calculations, for instance using the random phase approximation (RPA). The use of natural orbitals to compress the virtual space was shown to be effective, and would be a good starting point for making our basis more compact[98]. We note that it is also unclear whether our proposed bases

exhibit any scaling properties which will allow for higher accuracy by using basis set extrapolation for correlation energy calculations, which could be further investigated in the future.

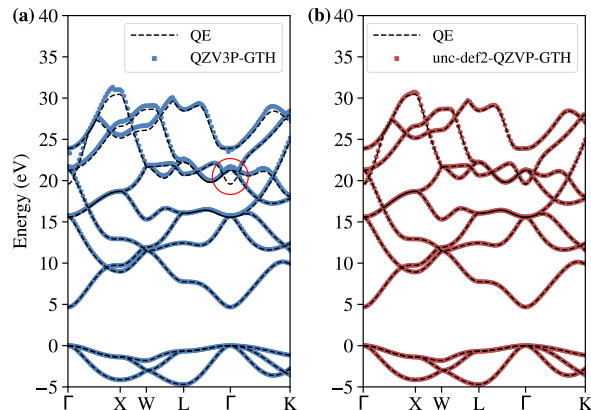## B. Even low-lying virtual orbitals can be difficult to describe well

FIG. 6. LDA band structure of MgO: (a) comparing QZV3P-GTH against QE and (b) comparing unc-def2-QZVP-GTH against QE. The band energies are shifted such that the highest valence band energy is located at zero. The red circle in (a) highlights the qualitative failure of QZV3P-GTH virtual orbitals.

Basis sets that are optimized for mean-field calculations such as GTH bases often behave erratically in correlated calculations.[19] Since these bases tend to yield good occupied orbitals, the poor performance of correlation calculations can be attributed to virtual orbitals. Furthermore, low-lying virtual orbitals play important roles in describing optical properties and related excited states. Therefore, high-quality basis sets should produce qualitatively accurate virtuals. As an example, we present the band structure of MgO using QZV3P-GTH and unc-def2-QZVP-GTH and compare them against that of QE. MgO has a total of 8 occupied orbitals and we computed up to the 16-th band in QE for comparison purposes. We note that the challenge of MgO conduction bands for GTOs was noted before in ref. [99], but we focus on a wider range of conduction bands here. The pertinent band structures are presented in Fig. 6.

In both bases, the valence bands and the first few conduction bands are in an excellent agreement with those of QE. However, the higher-lying virtuals of QZV3P-GTH (in Fig. 6(a)) start to deviate significantly from those of QE. The most striking failure is the lack of the 5-th virtual orbital highlighted under a red circle in Fig. 6 (a). On the other hand, the virtuals from unc-def2-QZVP-GTH have visually indistinguishable energies when compared to QE highlighting its potential utility for correlated calculations as well. We also tried a smaller

unc-def2-GTH basis set, namely unc-def2-TZVP-GTH. It turns out that even unc-def2-TZVP-GTH misses the same virtual that QZV3P-GTH misses as well. With further investigations, we found that the 5-th virtual orbital is missed by basis sets without any f function on the Mg atom. To be more concrete, we added one f-function to Mg in the QZV3P-GTH basis where the exponent of 0.16 was taken from unc-def2-QZVP-GTH. With this basis set, we recover the missing band at the Γ-point. This additional f-function introduces only a 0.2 mE_h energy lowering in the ground state, but it is essential to capture one of the low-lying conduction bands.

This example emphasizes that more attention to the low-lying virtual orbitals should be paid when designing GTO basis sets for applications such as conduction band structure, time-dependent DFT and correlated methods such as RPA. Existing GTO bases designed primarily to describe the occupied space may likewise exhibit qualitative failures like this case.

C. Transferability across different lattice constants is challenging

Cold curves of solids are often of great interest for experimentalists. Cold curves are analogous to potential energy curves (PECs) in molecular quantum chemistry. Similar to PECs, as one shrinks the lattice constant and brings atoms close to one another, a larger number of near linear dependencies occur, and the quality of the underlying GTO basis degrades because of discarding such functions by canonical orthogonalization. Furthermore, system-dependent optimization strategies can struggle for cold curves because basis sets are usually optimized for one specific geometry (usually equilibrium geometries).[19,20] As a result of this, varying lattice constants can be challenging using GTO basis sets as the system approaches its high-pressure configuration (shorter lattice constants) or atomic limits (longer lattice constants).

As an example to illustrate this point, we computed a cold curve of SiC using PBE and the GTH-LDA pseudopotential with TZV2P-GTH, QZV3P-GTH, unc-QZV3P-GTH, unc-def2-TZVP, and unc-def2-QZVP. The Brillouin zone was sampled with $6 \times 6 \times 6$ **k**-points via the Monkhorst-Pack algorithm. Here unc-QZV3P-GTH is the basis obtained from decontracting QZV3P-GTH. Using unc-QZV3P-GTH, we can quantify the error coming from the contraction coefficients of QZV3P-GTH. As before, the QE results (the same functional and pseudopotential) serve as the basis set limit reference values. The pertinent results are presented in Fig. 7.

Fig. 7 (a) shows that TZV2P-GTH, QZV3P-GTH, and unc-QZV3P-GTH bases make a large error especially when compressing the lattice. It is also instructive to quantify the nonparallelity error (NPE) over the range of lattice constants examined here as a means to measure error cancellation. The NPE is 25.7 mE_h, 10.6
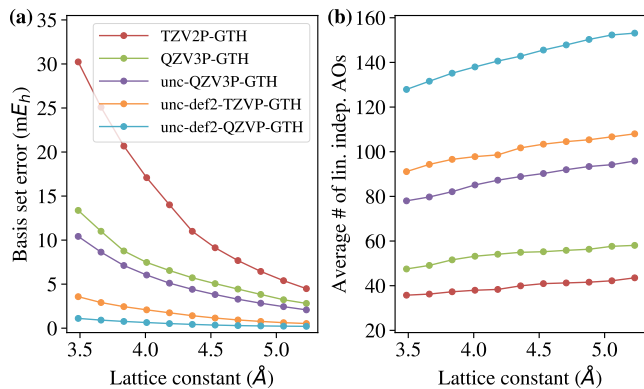
FIG. 7. Investigation of a SiC cold curve using PBE: (a) Basis set error with respect to QE as a function of lattice constant for various basis sets. (b) Average number of linearly independent AOs as a function of the lattice constant for various basis sets.

mE_h, 8.3 mE_h, 3.0 mE_h, and 0.9 mE_h, respectively, for TZV2P-GTH, QZV3P-GTH, unc-QZV3P-GTH, unc-def2-TZVP-GTH, and unc-def2-QZVP-GTH. Interestingly, unc-QZV3P-GTH reduces the basis set error by only a small amount, which implies that the contraction coefficients of QZV3P-GTH for those elements are transferable over a wide range of lattice constants. It also suggests that the range of exponents in QZV3P-GTH becomes inappropriate for smaller lattice constants. Comparing the exponents of unc-QZV3P-GTH and unc-def2-TZVP-GTH, we find that unc-def2-TZVP-GTH has more compact exponents for spd shells and has an f shell for Si that is not present in unc-QZV3P-GTH. These more compact GTOs likely become more important at closer distances and hence explain the differences between two bases.

The main cause of these generally large NPEs is the fact that at closer distances the quality of those GTO bases degrades as shown in Fig. 7 (b) which quantifies the number of orthogonalized basis functions retained after canonical orthogonalization. Since each **k**-point has a slightly different number of linearly independent AOs, we present the average values over 216 **k**-points as a function of lattice constant. Evidently, the number of linearly independent AOs decreases as the lattice constant decreases, which in turn increases the basis set incompleteness error. Nonetheless, the largest basis set, unc-def2-QZVP-GTH, is able to achieve a satisfying NPE in this case, which highlights the utility of this basis set for accurate cold curve simulations.

VI. CONCLUSIONS

In this manuscript, we discussed strategies for generating large and accurate uncontracted Gaussian bases (unc-def2-GTH bases) which do not resort to system-

or method- specific optimizations. Using a new implementation of the Gaussian atomic orbital plus planewave density fitting approach in Q-Chem, the basis set incompleteness error in our proposed bases were then assessed over 43 prototypical semiconductors by comparing the pure density functional theory total energies per cell and band gaps against those from fully converged planewave results. We found that the basis set incompleteness error in total energy and band gap with our largest GTO basis (unc-def2-QZVP-GTH) is smaller than 0.7 mE_h per atom in the unit cell and less than 20 meV, respectively, verifying the validity of the range of exponents and angular momenta in the proposed bases.

In the application of our bases, we focused on the assessment of ten pure density functionals for predicting the band gaps of 36 semiconductors whose experimental gaps are well documented. Not surprisingly, we found that all examined pure functionals (LDA, PBE, PBEsol, revPBE, BLYP, B97-D, SCAN, M06-L, MN15-L, B97M-rV) significantly underestimate the band gaps of these materials. The combinatorially optimized mGGA functional, B97M-rV, performs as well as do other modern mGGA functionals. Our work suggests that combinatorially optimized range-separated hybrid functionals such as ωB97X-rV and ωB97M-rV will be highly interesting to study since they may also exhibit better accuracy compared to other relatively older range-separated hybrid functionals or even short-range hybrid functionals.

We also made several cautionary remarks on our GTO bases as well as on the future research in GTO basis design for solids:

1. Our basis sets are accurate but large so there is a need for a way to compress our basis sets further for both mean-field and correlation calculations.

2. The widely used GTH bases may qualitatively fail for describing low-lying virtual orbitals which will affect the subsequent correlation and optical calculations. At much greater compute cost, our unc-def2-QZVP-GTH basis set was shown to accurately capture all of the low-lying virtual orbitals of MgO including the one missed by QZV3P-GTH.

3. Reducing the non-parallelity error of the basis set incompleteness error is challenging particularly due to the high pressure region of cold curves that exhibits a higher number of near linear dependencies.

In the future, we will test several ways (e.g., finding universal contraction coefficients and frozen natural orbitals[98]) to compress our unc-def2-GTH bases and investigate the basis set convergence of correlation and optical methods with these bases in the future. Furthermore, simple solids like LiH have many numerical data of the total Hartree-Fock energies towards the basis set limit,[100–104] which could be a good testbed for our basis sets in the future.

VII. SUPPLEMENTARY MATERIAL

The supplementary material of this work is available, which contains the test of the impact of different GTH pseudopotentials in the band gaps.

VIII. ACKNOWLEDGEMENT

IX. DATA AVAILABILITY STATEMENT

The data that supports the findings of this study are available within the article and its supplementary material.

X. CONFLICT OF INTEREST

E.E. and M.H.-G. are part-owners of Q-Chem, Inc.

[1] Philippe Y. Ayala, Konstantin N. Kudin, and Gustavo E. Scuseria, "Atomic orbital Laplace-transformed second-order Møller–Plesset theory for periodic systems," J. Chem. Phys. **115**, 9698–9707 (2001).

[2] Hideki Katagiri, "Equation-of-motion coupled-cluster study on exciton states of polyethylene with periodic boundary condition," J. Chem. Phys. **122**, 224901 (2005).

[3] Artur F. Izmaylov and Gustavo E. Scuseria, "Resolution of the identity atomic orbital Laplace transformed second order Møller–Plesset theory for nonconducting periodic systems," Phys. Chem. Chem. Phys. **10**, 3421–3429 (2008).

[4] Cesare Pisani, Lorenzo Maschio, Silvia Casassa, Migen Halo, Martin Schütz, and Denis Usvyat, "Periodic local MP2 method for the study of electronic correlation in crystals: Theory and preliminary applications," J. Comput. Chem. **29**, 2113–2124 (2008).

[5] Cesare Pisani, Martin Schütz, Silvia Casassa, Denis Usvyat, Lorenzo Maschio, Marco Lorenz, and Alessandro Erba, "C ryscor : a program for the post-Hartree–Fock treatment of periodic systems," Phys. Chem. Chem. Phys. **14**, 7615–7628 (2012).

[6] Mauro Del Ben, Jürg Hutter, and Joost VandeVondele, "Second-Order Møller–Plesset Perturbation Theory in the Condensed Phase: An Efficient and Massively Parallel Gaussian and Plane Waves Approach," J. Chem. Theory Comput. **8**, 4177–4188 (2012).

[7] Denis Usvyat, Lorenzo Maschio, and Martin Schütz, "Periodic local MP2 method employing orbital specific virtuals," J. Chem. Phys. **143**, 102805 (2015).

[8] James McClain, Qiming Sun, Garnet Kin-Lic Chan, and Timothy C. Berkelbach, "Gaussian-Based Coupled-Cluster Theory for the Ground-State and Band Structure of Solids," J. Chem. Theory Comput. **13**, 1209–1218 (2017).

[9] Honghui Shang and Jinlong Yang, "Implementation of Laplace Transformed MP2 for Periodic Systems With Numerical Atomic Orbitals," Front. Chem. **8** (2020), 10.3389/fchem.2020.589992.

[10] Reinhard J. Maurer, Christoph Freysoldt, Anthony M. Reilly, Jan Gerit Brandenburg, Oliver T. Hofmann, Torbjörn Björkman, Sébastien Lebègue, and Alexandre Tkatchenko, "Advances in Density-Functional Calculations for Materials Modeling," Annu. Rev. Mater. Res. **49**, 1–30 (2019).

[11] Mark S. Hybertsen and Steven G. Louie, "Electron correlation in semiconductors and insulators: Band gaps and quasiparticle energies," Phys. Rev. B **34**, 5390–5413 (1986).

[12] F. Aryasetiawan and O. Gunnarsson, "The GW method," Rep. Prog. Phys. **61**, 237–312 (1998).

[13] Per-Olov Löwdin, "On the Nonorthogonality Problem," in Advances in Quantum Chemistry, Vol. 5 (Academic Press, Cambridge, MA, USA, 1970) pp. 185–199.

[14] Bruno Klahn and Werner A. Bingel, "Completeness and linear independence of basis sets used in quantum chemistry," Int. J. Quantum Chem. **11**, 943–957 (1977).

[15] Joost VandeVondele and Jürg Hutter, "Gaussian basis sets for accurate calculations on molecular systems in gas and condensed phases," J. Chem. Phys. **127**, 114105 (2007).

[16] Michael F. Peintinger, Daniel Vilela Oliveira, and Thomas Bredow, "Consistent Gaussian basis sets of triple-zeta valence with polarization quality for solid-state calculations," J. Comput. Chem. **34**, 451–459 (2013).

[17] Joachim Laun, Daniel Vilela Oliveira, and Thomas Bredow, "Consistent gaussian basis sets of double- and triple-zeta valence with polarization quality of the fifth period for solid-state calculations," J. Comput. Chem. **39**, 1285–1290 (2018).

[18] Daniel Vilela Oliveira, Joachim Laun, Michael F. Peintinger, and Thomas Bredow, "BSSE-correction scheme for consistent gaussian basis sets of double- and triple-zeta valence with polarization quality for solid-state calculations," J. Comput. Chem. **40**, 2364–2376 (2019).

[19] Miguel A. Morales and Fionn D. Malone, "Accelerating the convergence of auxiliary-field quantum Monte Carlo in solids with optimized Gaussian basis sets," J. Chem. Phys. **153**, 194111 (2020).

[20] Loredana Edith Daga, Bartolomeo Civalleri, and Lorenzo Maschio, "Gaussian Basis Sets for Crystalline Solids: All-Purpose Basis Set Libraries vs System-Specific Optimizations," J. Chem. Theory Comput. **16**, 2192–2201 (2020).

[21] Yanbing Zhou, Emanuel Gull, and Dominika Zgid, "Material-Specific Optimization of Gaussian Basis Sets against Plane Wave Data," J. Chem. Theory Comput. **17**, 5611–5622 (2021).

[22] Y. S. Li, M. C. Wrinn, J. M. Newsam, and M. P. Sears, "Parallel implementation of a mesh-based density functional electronic structure code," J. Comput. Chem. **16**, 226–234 (1995).

[23] José M. Soler, Emilio Artacho, Julian D. Gale, Alberto García, Javier Junquera, Pablo Ordejón, and Daniel Sánchez-Portal, "The SIESTA method for ab initio order-N," J. Phys.: Condens. Matter **14**, 2745–2779 (2002).

[24] Emilio Artacho, E. Anglada, O. Diéguez, J. D. Gale, A. García, J. Junquera, R. M. Martin, P. Ordejón, J. M. Pruneda, D. Sánchez-Portal, and J. M. Soler, "The SIESTA method; developments and applicability," J. Phys.: Condens. Matter **20**, 064208 (2008).

[25] C. J. O. Verzijl and J. M. Thijssen, "DFT-Based Molecular Transport Implementation in ADF/BAND," J. Phys. Chem. C **116**, 24393–24412 (2012).

[26] Konstantin N. Kudin and Gustavo E. Scuseria, "Linear-scaling density-functional theory with Gaussian orbitals and periodic boundary conditions: Efficient evaluation of energy and forces via the fast multipole method," Phys. Rev. B **61**, 16440–16453 (2000).

[27] Sree Ganesh Balasubramani, Guo P. Chen, Sonia Coriani, Michael Diedenhofen, Marius S. Frank, Yannick J. Franzke, Filipp Furche, Robin Grotjahn, Michael E. Harding, Christof Hättig, Arnim Hellweg, Benjamin Helmich-Paris, Christof Holzer, Uwe Huniar, Martin Kaupp, Alireza Marefat Khah, Sarah Karbalaei Khani, Thomas Müller, Fabian Mack, Brian D. Nguyen, Shane M. Parker, Eva Perlt, Dmitrij Rappoport, Kevin

Reiter, Saswata Roy, Matthias Rückert, Gunnar Schmitz, Marek Sierka, Enrico Tapavicza, David P. Tew, Christoph van Wüllen, Vamsee K. Voora, Florian Weigend, Artur Wodyński, and Jason M. Yu, "TURBOMOLE: Modular program suite for ab initio quantum-chemical and condensed-matter simulations," J. Chem. Phys. **152**, 184107 (2020).

[28] Roberto Dovesi, Fabien Pascale, Bartolomeo Civalleri, Klaus Doll, Nicholas M. Harrison, Ian Bush, Philippe D'Arco, Yves Noël, Michel Rérat, Philippe Carbonnière, Mauro Causà, Simone Salustro, Valentina Lacivita, Bernard Kirtman, Anna Maria Ferrari, Francesco Silvio Gentile, Jacopo Baima, Mauro Ferrero, Raffaella Demichelis, and Marco De La Pierre, "The CRYSTAL code, 1976–2020 and beyond, a long story," J. Chem. Phys. **152**, 204111 (2020).

[29] Thomas D. Kühne, Marcella Iannuzzi, Mauro Del Ben, Vladimir V. Rybkin, Patrick Seewald, Frederick Stein, Teodoro Laino, Rustam Z. Khaliullin, Ole Schütt, Florian Schiffmann, Dorothea Golze, Jan Wilhelm, Sergey Chulkov, Mohammad Hossein Bani-Hashemian, Valéry Weber, Urban Borštnik, Mathieu Taillefumier, Alice Shoshana Jakobovits, Alfio Lazzaro, Hans Pabst, Tiziano Müller, Robert Schade, Manuel Guidon, Samuel Andermatt, Nico Holmberg, Gregory K. Schenter, Anna Hehn, Augustin Bussy, Fabian Belleflamme, Gloria Tabacchi, Andreas Glöß, Michael Lass, Iain Bethune, Christopher J. Mundy, Christian Plessl, Matt Watkins, Joost VandeVondele, Matthias Krack, and Jürg Hutter, "CP2K: An electronic structure and molecular dynamics software package - Quickstep: Efficient and accurate electronic structure calculations," J. Chem. Phys. **152**, 194103 (2020).

[30] Joseph C. A. Prentice, Jolyon Aarons, James C. Womack, Alice E. A. Allen, Lampros Andrinopoulos, Lucian Anton, Robert A. Bell, Arihant Bhandari, Gabriel A. Bramley, Robert J. Charlton, Rebecca J. Clements, Daniel J. Cole, Gabriel Constantinescu, Fabiano Corsetti, Simon M.-M. Dubois, Kevin K. B. Duff, José María Escartín, Andrea Greco, Quintin Hill, Louis P. Lee, Edward Linscott, David D. O'Regan, Maximillian J. S. Phipps, Laura E. Ratcliff, Álvaro Ruiz Serrano, Edward W. Tait, Gilberto Teobaldi, Valerio Vitale, Nelson Yeung, Tim J. Zuehlsdorff, Jacek Dziedzic, Peter D. Haynes, Nicholas D. M. Hine, Arash A. Mostofi, Mike C. Payne, and Chris-Kriton Skylaris, "The ONETEP linear-scaling density functional theory program," J. Chem. Phys. **152**, 174111 (2020).

[31] Frank Jensen, "Atomic orbital basis sets," WIRES: Comput. Mol. Sci. **3**, 273–295 (2013).

[32] Balazs Nagy and Frank Jensen, "Basis sets in quantum chemistry," Rev. Computat. Chem. **30**, 93–149 (2017).

[33] Isaiah Shavitt, "The History and Evolution of Gaussian Basis Sets," Isr. J. Chem. **33**, 357–367 (1993).

[34] Benjamin P. Pritchard, Doaa Altarawy, Brett Didier, Tara D. Gibson, and Theresa L. Windus, "New Basis Set Exchange: An Open, Up-to-Date Resource for the Molecular Sciences Community," J. Chem. Inf. Model. **59**, 4814–4820 (2019).

[35] R. Mcweeny, "Gaussian Approximations, to Wave Functions - Nature," Nature **166**, 21–22 (1950).

[36] F. Boys S., "Electronic wave functions - I. A general method of calculation for the stationary states of any molecular system," Proc. R. Soc. London A - Math. Phys. Sci. **200**, 542–554 (1950).

[37] Jan Almlöf and Peter R. Taylor, "General contraction of Gaussian basis sets. I. Atomic natural orbitals for first- and second-row atoms," J. Chem. Phys. **86**, 4070–4077 (1987).

[38] Thom H. Dunning, "Gaussian basis sets for use in correlated molecular calculations. I. The atoms boron through neon and hydrogen," J. Chem. Phys. **90**, 1007–1023 (1989).

[39] Frank Jensen, "Polarization consistent basis sets: Principles," J. Chem. Phys. **115**, 9113–9125 (2001).

[40] Frank Jensen, "Polarization consistent basis sets. ii. estimating the kohn–sham basis set limit," J. Chem. Phys. **116**, 7372–7379 (2002).

[41] Richard D. Bardo and Klaus Ruedenberg, "Even-tempered atomic orbitals. III. Economic deployment of Gaussian primitives in expanding atomic SCF orbitals," J. Chem. Phys. **59**, 5956–5965 (1973).

[42] David F. Feller and Klaus Ruedenberg, "Systematic approach to extended even-tempered orbital bases for atomic and molecular calculations," Theor. Chim. Acta **52**, 231–251 (1979).

[43] S. Huzinaga, M. Klobukowski, and H. Tatewaki, "The well-tempered GTF basis sets and their applications in the SCF calculations on N2, CO, Na2, and P2," Can. J. Chem. **63**, 1812 (1985).

[44] Florian Weigend and Reinhart Ahlrichs, "Balanced basis sets of split valence, triple zeta valence and quadruple zeta valence quality for H to Rn: Design and assessment of accuracy," Phys. Chem. Chem. Phys. **7**, 3297–3305 (2005).

[45] S. Goedecker, M. Teter, and J. Hutter, "Separable dual-space Gaussian pseudopotentials," Phys. Rev. B **54**, 1703–1710 (1996).

[46] C. Hartwigsen, S. Goedecker, and J. Hutter, "Relativistic separable dual-space Gaussian pseudopotentials from H to Rn," Phys. Rev. B **58**, 3641–3662 (1998).

[47] Paolo Giannozzi, Oscar Baseggio, Pietro Bonfà, Davide Brunato, Roberto Car, Ivan Carnimeo, Carlo Cavazzoni, Stefano De Gironcoli, Pietro Delugas, Fabrizio Ferrari Ruffino, et al., "Quantum espresso toward the exascale," J. Chem. Phys. **152**, 154105 (2020).

[48] John C Slater, "A simplification of the hartree-fock method," Phys. Rev. **81**, 385 (1951).

[49] John P Perdew and Alex Zunger, "Self-interaction correction to density-functional approximations for many-electron systems," Phys. Rev. B **23**, 5048 (1981).

[50] John P Perdew, Kieron Burke, and Matthias Ernzerhof, "Generalized gradient approximation made simple," Phys. Rev. Lett. **77**, 3865 (1996).

[51] John P. Perdew, Adrienn Ruzsinszky, Gábor I. Csonka, Oleg A. Vydrov, Gustavo E. Scuseria, Lucian A. Constantin, Xiaolan Zhou, and Kieron Burke, "Restoring the Density-Gradient Expansion for Exchange in Solids and Surfaces," Phys. Rev. Lett. **100**, 136406 (2008).

[52] Yingkai Zhang and Weitao Yang, "Comment on "Generalized Gradient Approximation Made Simple"," Phys. Rev. Lett. **80**, 890 (1998).

[53] Axel D Becke, "Density-functional exchange-energy approximation with correct asymptotic behavior," Phys. Rev. A **38**, 3098 (1988).

[54] Chengteh Lee, Weitao Yang, and Robert G Parr, "Development of the colle-salvetti correlation-energy formula into a functional of the electron density," Phys. Rev. B **37**, 785 (1988).

[55] Stefan Grimme, "Semiempirical GGA-type density functional constructed with a long-range dispersion correction," J. Comput. Chem. **27**, 1787–1799 (2006).

[56] Jianwei Sun, Adrienn Ruzsinszky, and John P Perdew, "Strongly constrained and appropriately normed semilocal density functional," Phys. Rev. Lett. **115**, 036402 (2015).

[57] Yan Zhao and Donald G. Truhlar, "A new local density functional for main-group thermochemistry, transition metal bonding, thermochemical kinetics, and noncovalent interactions," J. Chem. Phys. **125**, 194101 (2006).

[58] Haoyu S. Yu, Xiao He, and Donald G. Truhlar, "MN15-L: A New Local Exchange-Correlation Functional for Kohn–Sham Density Functional Theory with Broad Accuracy for Atoms, Molecules, and Solids," J. Chem. Theory Comput. **12**, 1280–1293 (2016).

[59] Narbe Mardirossian and Martin Head-Gordon, "Mapping the genome of meta-generalized gradient approximation density functionals: The search for b97m-v," J. Chem. Phys. **142**, 074111 (2015).

[60] Narbe Mardirossian, Luis Ruiz Pestana, James C Womack, Chris-Kriton Skylaris, Teresa Head-Gordon, and Martin Head-Gordon, "Use of the rvv10 nonlocal correlation functional in the b97m-v density functional: Defining b97m-rv and related functionals," J. Phys. Chem. Lett. **8**, 35–40 (2017).

[61] Jochen Heyd, Juan E Peralta, Gustavo E Scuseria, and Richard L Martin, "Energy band gaps and lattice parameters evaluated with the heyd-scuseria-ernzerhof screened hybrid functional," J. Chem. Phys. **123**, 174101 (2005).

[62] JEAN PIERRE Vidal and G Vidal-Valat, "Accurate debye–waller factors of 7lih and 7lid by neutron diffraction at three temperatures," Acta Crystallogr., Sect. B: Struct. Sci. **42**, 131–137 (1986).

[63] SJ Nolan, MJ Gillan, D Alfè, NL Allan, and FR Manby, "Calculation of properties of crystalline lithium hydride using correlated wave function theory," Phys. Rev. B **80**, 165109 (2009).

[64] Khang Hoang and Chris G Van de Walle, "Lih as a li+ and h-ion provider," Solid State Ion. **253**, 53–56 (2013).

[65] Yu-ichiro Matsushita, Kazuma Nakamura, and Atsushi Oshiyama, "Comparative study of hybrid functionals applied to structural and electronic properties of semiconductors and insulators," Phys. Rev. B **84**, 075205 (2011).

[66] Alejandro J Garza and Gustavo E Scuseria, "Predicting band gaps with hybrid density functionals," J. Phys. Chem. Lett. **7**, 4165–4170 (2016).

[67] John P Perdew, Weitao Yang, Kieron Burke, Zenghui Yang, Eberhard KU Gross, Matthias Scheffler, Gustavo E Scuseria, Thomas M Henderson, Igor Ying Zhang, Adrienn Ruzsinszky, *et al.*, "Understanding band gaps of solids in generalized kohn–sham theory," Proc. Natl. Acad. Sci. U.S.A **114**, 2801–2806 (2017).

[68] Zeng-hui Yang, Haowei Peng, Jianwei Sun, and John P Perdew, "More realistic band gaps from meta-generalized gradient approximations: Only in a generalized kohn-sham scheme," Phys. Rev. B **93**, 205205 (2016).

[69] Narbe Mardirossian and Martin Head-Gordon, "ωb97x-v: A 10-parameter, range-separated hybrid, generalized gradient approximation density functional with nonlocal correlation, designed by a survival-of-the-fittest strategy," Phys. Chem. Chem. Phys. **16**, 9904–9924 (2014).

[70] Narbe Mardirossian and Martin Head-Gordon, "ω b97m-v: A combinatorially optimized, range-separated hybrid, meta-gga density functional with vv10 nonlocal correlation," J. Chem. Phys. **144**, 214110 (2016).

[71] Luis Ruiz Pestana, Narbe Mardirossian, Martin Head-Gordon, and Teresa Head-Gordon, "Ab initio molecular dynamics simulations of liquid water using high quality meta-gga functionals," Chem. Sci. **8**, 3554–3565 (2017).

[72] Luis Ruiz Pestana, Ondrej Marsalek, Thomas E Markland, and Teresa Head-Gordon, "The quest for accurate liquid water properties from first principles," J. Phys. Chem. Lett. **9**, 5009–5016 (2018).

[73] Luis Ruiz Pestana, Hongxia Hao, and Teresa Head-Gordon, "Diels–alder reactions in water are determined by microsolvation," Nano Lett. **20**, 606–611 (2019).

[74] Christianna N Lininger, Joseph A Gauthier, Wan-Lu Li, Elliot Rossomme, Valerie Vaissier Welborn, Zhou Lin, Teresa Head-Gordon, Martin Head-Gordon, and Alexis T Bell, "Challenges for density functional theory: calculation of co adsorption on electrocatalytically relevant metals," Phys. Chem. Chem. Phys. **23**, 9394–9406 (2021).

[75] Wan-Lu Li, Christianna N Lininger, Kaixuan Chen, Valerie Vaissier Welborn, Elliot Rossomme, Alexis T Bell, Martin Head-Gordon, and Teresa Head-Gordon, "Critical role of thermal fluctuations for co binding on electrocatalytic metal surfaces," JACS Au , (in press) (2021).

[76] Riccardo Sabatini, Tommaso Gorni, and Stefano De Gironcoli, "Nonlocal van der waals density functional made simple and efficient," Phys. Rev. B **87**, 041108 (2013).

[77] Oleg A Vydrov and Troy Van Voorhis, "Nonlocal van der waals density functional: The simpler the better," J. Chem. Phys. **133**, 244103 (2010).

[78] Narbe Mardirossian and Martin Head-Gordon, "Thirty years of density functional theory in computational chemistry: an overview and extensive assessment of 200 density functionals," Mol. Phys. **115**, 2315–2372 (2017).

[79] L. Goerigk, A. Hansen, C. Bauer, S. Ehrlich, A. Najibi, and S. Grimme, "A look at the density functional theory zoo with the advanced GMTKN55 database for general main group thermochemistry, kinetics and noncovalent interactions," Phys. Chem. Chem. Phys. **19**, 32184–32215 (2017).

[80] A. Najibi and L. Goerigk, "The nonlocal kernel in van der Waals density functionals as an additive correction: An extensive analysis with special emphasis on the B97M-V and ωB97M-V approches," J. Chem. Theory Comput. **14**, 5725–5738 (2018).

[81] Robert Evarestov, *Quantum Chemistry of Solids* (Springer-Verlag, Berlin, Germany, 2007).

[82] R. A. Evarestov, *Quantum Chemistry of Solids* (Springer-Verlag, Berlin, Germany, 2012).

[83] Konstantin N Kudin and Gustavo E Scuseria, "A fast multipole algorithm for the efficient treatment of the coulomb problem in electronic structure calculations of periodic systems with gaussian orbitals," Chem. Phys. Lett. **289**, 611–616 (1998).

[84] Attila Szabo and Neil S. Ostlund, *Modern Quantum Chemistry: Introduction to Advanced Electronic Structure Theory* (Courier Corporation, 1996).

[85] Yihan Shao, Zhengting Gan, Evgeny Epifanovsky, Andrew T. B. Gilbert, Michael Wormit, Joerg Kussmann, Adrian W. Lange, Andrew Behn, Jia Deng, Xintian Feng, Debashree Ghosh, Matthew Goldey, Paul R. Horn, Leif D. Jacobson, Ilya Kaliman, Rustam Z. Khaliullin, Tomasz Kuś, Arie Landau, Jie Liu, Emil I. Proynov, Young Min Rhee, Ryan M. Richard, Mary A. Rohrdanz, Ryan P. Steele, Eric J. Sundstrom, H. Lee Woodcock, Paul M. Zimmerman, Dmitry Zuev, Ben Albrecht, Ethan Alguire, Brian Austin, Gregory J. O. Beran, Yves A. Bernard, Eric Berquist, Kai Brandhorst, Ksenia B. Bravaya, Shawn T. Brown, David Casanova, Chun-Min Chang, Yunqing Chen, Siu Hung Chien, Kristina D. Closser, Deborah L. Crittenden, Michael Diedenhofen, Robert A. DiStasio, Hainam Do, Anthony D. Dutoi, Richard G. Edgar, Shervin Fatehi, Laszlo Fusti-Molnar, An Ghysels, Anna Golubeva-Zadorozhnaya, Joseph Gomes, Magnus W. D. Hanson-Heine, Philipp H. P. Harbach, Andreas W. Hauser, Edward G. Hohenstein, Zachary C. Holden, Thomas-C. Jagau, Hyunjun Ji, Benjamin Kaduk, Kirill Khistyaev, Jaehoon Kim, Jihan Kim, Rollin A. King, Phil Klunzinger, Dmytro Kosenkov, Tim Kowalczyk, Caroline M. Krauter, Ka Un Lao, Adèle D. Laurent, Keith V. Lawler, Sergey V. Levchenko, Ching Yeh Lin, Fenglai Liu, Ester Livshits, Rohini C. Lochan, Arne Luenser, Prashant Manohar, Samuel F. Manzer, Shan-Ping Mao, Narbe Mardirossian, Aleksandr V. Marenich, Simon A. Maurer, Nicholas J. Mayhall, Eric Neuscamman, C. Melania Oana, Roberto Olivares-Amaya, Darragh P. O'Neill, John A. Parkhill, Trilisa M. Perrine, Roberto Peverati, Alexander Prociuk, Dirk R. Rehn, Edina Rosta, Nicholas J. Russ, Shaama M. Sharada, Sandeep Sharma, David W. Small, Alexander Sodt, Tamar Stein, David Stück, Yu-Chuan Su, Alex J. W. Thom, Takashi Tsuchimochi, Vitalii Vanovschi, Leslie Vogt, Oleg Vydrov, Tao Wang, Mark A. Watson, Jan Wenzel, Alec White, Christopher F. Williams, Jun Yang, Sina Yeganeh, Shane R. Yost, Zhi-Qiang You, Igor Ying Zhang, Xing Zhang, Yan Zhao, Bernard R. Brooks, Garnet K. L. Chan, Daniel M. Chipman, Christopher J. Cramer, William A. Goddard, Mark S. Gordon, Warren J. Hehre, Andreas Klamt, Henry F. Schaefer, Michael W. Schmidt, C. David Sherrill, Donald G. Truhlar, Arieh Warshel, Xin Xu, Alán Aspuru-Guzik, Roi Baer, Alexis T. Bell, Nicholas A. Besley, Jeng-Da Chai, Andreas Dreuw, Barry D. Dunietz, Thomas R. Furlani, Steven R. Gwaltney, Chao-Ping Hsu, Yousung Jung, Jing Kong, Daniel S. Lambrecht, WanZhen Liang, Christian Ochsenfeld, Vitaly A. Rassolov, Lyudmila V. Slipchenko, Joseph E. Subotnik, Troy Van Voorhis, John M. Herbert, Anna I. Krylov, Peter M. W. Gill, and Martin Head-Gordon, "Advances in molecular quantum chemistry contained in the Q-Chem 4 program package," Mol. Phys. **113**, 184–215 (2015).

[86]Evgeny Epifanovsky, Andrew T. B. Gilbert, Xintian Feng, Joonho Lee, Yuezhi Mao, Narbe Mardirossian, Pavel Pokhilko, Alec F. White, Marc P. Coons, Adrian L. Dempwolff, Zhengting Gan, Diptarka Hait, Paul R. Horn, Leif D. Jacobson, Ilya Kaliman, Jörg Kussmann, Adrian W. Lange, Ka Un Lao, Daniel S. Levine, Jie Liu, Simon C. McKenzie, Adrian F. Morrison, Kaushik D. Nanda, Felix Plasser, Dirk R. Rehn, Marta L. Vidal, Zhi-Qiang You, Ying Zhu, Bushra Alam, Benjamin J. Albrecht, Abdulrahman Aldossary, Ethan Alguire, Josefine H. Andersen, Vishikh Athavale, Dennis Barton, Khadiza Begam, Andrew Behn, Nicole Bellonzi, Yves A. Bernard, Eric J. Berquist, Hugh G. A. Burton, Abel Carreras, Kevin Carter-Fenk, Romit Chakraborty, Alan D. Chien, Kristina D. Closser, Vale Cofer-Shabica, Saswata Dasgupta, Marc de Wergifosse, Jia Deng, Michael Diedenhofen, Hainam Do, Sebastian Ehlert, Po-Tung Fang, Shervin Fatehi, Qingguo Feng, Triet Friedhoff, James Gayvert, Qinghui Ge, Gergely Gidofalvi, Matthew Goldey, Joe Gomes, Cristina E. González-Espinoza, Sahil Gulania, Anastasia O. Gunina, Magnus W. D. Hanson-Heine, Phillip H. P. Harbach, Andreas Hauser, Michael F. Herbst, Mario Hernández Vera, Manuel Hodecker, Zachary C. Holden, Shannon Houck, Xunkun Huang, Kerwin Hui, Bang C. Huynh, Maxim Ivanov, Ádám Jász, Hyunjun Ji, Hanjie Jiang, Benjamin Kaduk, Sven Kähler, Kirill Khistyaev, Jaehoon Kim, Gergely Kis, Phil Klunzinger, Zsuzsanna Koczor-Benda, Joong Hoon Koh, Dimitri Kosenkov, Laura Koulias, Tim Kowalczyk, Caroline M. Krauter, Karl Kue, Alexander Kunitsa, Thomas Kus, István Ladjánszki, Arie Landau, Keith V. Lawler, Daniel Lefrancois, Susi Lehtola, Run R. Li, Yi-Pei Li, Jiashu Liang, Marcus Liebenthal, Hung-Hsuan Lin, You-Sheng Lin, Fenglai Liu, Kuan-Yu Liu, Matthias Loipersberger, Arne Luenser, Aaditya Manjanath, Prashant Manohar, Erum Mansoor, Sam F. Manzer, Shan-Ping Mao, Aleksandr V. Marenich, Thomas Markovich, Stephen Mason, Simon A. Maurer, Peter F. McLaughlin, Maximilian F. S. J. Menger, Jan-Michael Mewes, Stefanie A. Mewes, Pierpaolo Morgante, J. Wayne Mullinax, Katherine J. Oosterbaan, Garrette Paran, Alexander C. Paul, Suranjan K. Paul, Fabijan Pavošević, Zheng Pei, Stefan Prager, Emil I. Proynov, Ádám Rák, Eloy Ramos-Cordoba, Bhaskar Rana, Alan E. Rask, Adam Rettig, Ryan M. Richard, Fazle Rob, Elliot Rossomme, Tarek Scheele, Maximilian Scheurer, Matthias Schneider, Nickolai Sergueev, Shaama M. Sharada, Wojciech Skomorowski, David W. Small, Christopher J. Stein, Yu-Chuan Su, Eric J. Sundstrom, Zhen Tao, Jonathan Thirman, Gábor J. Tornai, Takashi Tsuchimochi, Norm M. Tubman, Srimukh Prasad Veccham, Oleg Vydrov, Jan Wenzel, Jon Witte, Atsushi Yamada, Kun Yao, Sina Yeganeh, Shane R. Yost, Alexander Zech, Igor Ying Zhang, Xing Zhang, Yu Zhang, Dmitry Zuev, Alán Aspuru-Guzik, Alexis T. Bell, Nicholas A. Besley, Ksenia B. Bravaya, Bernard R. Brooks, David Casanova, Jeng-Da Chai, Sonia Coriani, Christopher J. Cramer, György Cserey, A. Eugene DePrince, Robert A. DiStasio, Andreas Dreuw, Barry D. Dunietz, Thomas R. Furlani, William A. Goddard, Sharon Hammes-Schiffer, Teresa Head-Gordon, Warren J. Hehre, Chao-Ping Hsu, Thomas-C. Jagau, Yousung Jung, Andreas Klamt, Jing Kong, Daniel S. Lambrecht, WanZhen Liang, Nicholas J. Mayhall, C. William McCurdy, Jeffrey B. Neaton, Christian Ochsenfeld, John A. Parkhill, Roberto Peverati, Vitaly A. Rassolov, Yihan Shao, Lyudmila V. Slipchenko, Tim Stauch, Ryan P. Steele, Joseph E. Subotnik, Alex J. W. Thom, Alexandre Tkatchenko, Donald G. Truhlar, Troy Van Voorhis, Tomasz A. Wesolowski, K. Birgitta Whaley, H. Lee Woodcock, Paul M. Zimmerman, Shirin Faraji, Peter M. W. Gill, Martin Head-Gordon, John M. Herbert, and Anna I. Krylov, "Software for the frontiers of quantum chemistry: An overview of developments in the Q-Chem 5 package," J. Chem. Phys. **155**, 084801 (2021).

[87]Gerald Lippert, Jürg Hutter, and Michele Parrinello, "A hybrid gaussian and plane wave density functional scheme," Mol. Phys. **92**, 477–488 (1997).

[88]Joost VandeVondele, Matthias Krack, Fawzi Mohamed, Michele Parrinello, Thomas Chassaing, and Jürg Hutter, "Quickstep: Fast and accurate density functional calculations using a mixed gaussian and plane waves approach," Comput. Phys. Commun. **167**, 103–128 (2005).

[89]László Füsti-Molnar and Peter Pulay, "Accurate molecular integrals and energies using combined plane wave and Gaussian basis sets in molecular electronic structure theory," J. Chem. Phys. **116**, 7795–7805 (2002).

[90]László Füsti-Molnár and Peter Pulay, "The Fourier transform Coulomb method: Efficient and accurate calculation of the Coulomb operator in a Gaussian basis," J. Chem. Phys. **117**, 7827–7835 (2002).

[91]Carlo A. Rozzi, Daniele Varsano, Andrea Marini, Eberhard K. U. Gross, and Angel Rubio, "Exact Coulomb cutoff technique for supercell calculations," Phys. Rev. B **73**, 205119 (2006).

[92]Guillermo Román-Pérez and José M Soler, "Efficient implementation of a van der waals density functional: application to double-wall carbon nanotubes," Phys. Rev. Lett. **103**, 096102 (2009).

[93]"Data repository for 'approaching the basis set limit in gaussian-orbital-based periodic calculations with transferability: Performance of pure density functionals for simple semiconductors'," (2021).

[94]Hendrik J Monkhorst and James D Pack, "Special points for brillouin-zone integrations," Phys. Rev. B **13**, 5188 (1976).

[95]Qiming Sun, Xing Zhang, Samragni Banerjee, Peng Bao, Marc Barbry, Nick S Blunt, Nikolay A Bogdanov, George H Booth, Jia Chen, Zhi-Hao Cui, *et al.*, "Recent developments in the pyscf program package," J. Chem. Phys. **153**, 024109 (2020).

[96]Narbe Mardirossian and Martin Head-Gordon, "Characterizing and understanding the remarkably slow basis set convergence of several minnesota density functionals for intermolecular interaction energies," J. Chem. Theory Comput. **9**, 4453–4461 (2013).

[97]Bartolomeo Civalleri, Davide Presti, Roberto Dovesi, and Andreas Savin, "On choosing the best density functional approximation," in *Chemical Modelling: Applications and Theory Volume 9*, Vol. 9 (The Royal Society of Chemistry, 2012) pp. 168–185.

[98]Benjamin Ramberger, Zoran Sukurma, Tobias Schäfer, and Georg Kresse, "Rpa natural orbitals and their application to post-hartree-fock electronic structure methods," J. Chem. Phys. **151**, 214106 (2019).

[99]Andreas Irmler, Asbjörn Burow, and Fabian Pauly, "Robust Periodic Fock Exchange with Atom-Centered Gaussian Basis Sets," J. Chem. Theory Comput. **14**, 4567–4580 (2018).

[100]M. J. Gillan, D. Alfè, S. de Gironcoli, and F. R. Manby, "High-precision calculation of Hartree-Fock energy of crystals," J. Comput. Chem. **29**, 2098–2106 (2008).

[101]M. Marsman, A. Grüneis, J. Paier, and G. Kresse, "Second-order Møller–Plesset perturbation theory applied to extended systems. I. Within the projector-augmented-wave formalism using a plane wave basis set," J. Chem. Phys. **130**, 184103 (2009).

[102]Joachim Paier, Cristian V. Diaconu, Gustavo E. Scuseria, Manuel Guidon, Joost VandeVondele, and Jürg Hutter, "Accurate Hartree-Fock energy of extended systems using large Gaussian basis sets," Phys. Rev. B **80**, 174114 (2009).

[103]Bartolomeo Civalleri, Roberto Orlando, Claudio M. Zicovich-Wilson, Carla Roetti, Victor R. Saunders, Cesare Pisani, and Roberto Dovesi, "Comment on "Accurate Hartree-Fock energy of extended systems using large Gaussian basis sets"," Phys. Rev. B **81**, 106101 (2010).

[104]Denis Usvyat, Bartolomeo Civalleri, Lorenzo Maschio, Roberto Dovesi, Cesare Pisani, and Martin Schütz, "Approaching the theoretical limit in periodic local MP2 calculations with atomic-orbital basis sets: The case of LiH," J. Chem. Phys. **134**, 214105 (2011).